Turun yliopisto
University of Turku

VASCULAR ADHESION PROTEIN-1 AS *IN VIVO* TARGET FOR IMAGING OF LEUKOCYTE TRANSENDOTHELIAL MIGRATION IN INFLAMMATION

Helena Virtanen née Ahtinen

Turun yliopisto
University of Turku

VASCULAR ADHESION PROTEIN-1 AS *IN VIVO* TARGET FOR IMAGING OF LEUKOCYTE TRANSENDOTHELIAL MIGRATION IN INFLAMMATION

Helena Virtanen née Ahtinen

University of Turku

Faculty of Medicine
Institute of Clinical Medicine
Department of Clinical Physiology and Nuclear Medicine
Drug Research Doctoral Programme at University of Turku
Turku PET Centre
Turku, Finland

Supervised by

Professor Anne Roivainen, PhD
Turku PET Centre and
Turku Center for Disease Modeling
University of Turku
Turku, Finland

Academy Professor Sirpa Jalkanen, MD, PhD
MediCity Research Laboratory
University of Turku
Turku, Finland

Reviewed by

Adjunct Professor, Kirsi Timonen, MD, PhD
Clinical Physiology and Nuclear Medicine
Central Finland Health Care District
Jyväskylä, Finland

Professor Aapo Ahonen, MD, PhD
Department of Clinical Physiology and
Nuclear Medicine,
Helsinki University Central Hospital
Helsinki, Finland

Opponent

Professor Risto Renkonen, MD, PhD
University of Helsinki
Helsinki, Finland

The originality of this thesis has been checked in accordance with the University of Turku quality assurance system using the Turnitin OriginalityCheck service.

To Juha-Pekka

ABSTRACT

Helena Virtanen née Ahtinen

VASCULAR ADHESION PROTEIN-1 AS IN VIVO TARGET FOR IMAGING OF LEUKOCYTE TRANSENDOTHELIAL MIGRATION IN INFLAMMATION

University of Turku, Faculty of Medicine, Department of Clinical Physiology and Nuclear Medicine, Drug Research Doctoral Programme, Turku PET Centre, Turku, Finland

Inflammation is related to many diseases, such as atherosclerosis, rheumatoid arthritis and metabolic diseases. Vascular adhesion protein-1 (VAP-1) is an endothelial adhesion molecule involved in leukocyte trafficking cascades from blood circulation to the sites of inflammation. In normal condition, VAP-1 is stored in intracellular granules. During inflammation it is rapidly translocated from the intracellular storage granules to the endothelial cell surface. Siglec-9 is a leukocyte ligand of VAP-1 and Siglec-9 motif containing peptide can be used as a positron emission tomography (PET) tracer for *in vivo* imaging of inflammation-related diseases.

For this study, radiolabeled Siglec-9 was evaluated for feasibility as a tracer in imaging orthopaedic implant infection in rats, synovitis in rabbits, turpentine oil-induced inflammation in rats and atherosclerosis in mice. Dynamic PET imaging was performed using [^{68}Ga]DOTA-Siglec-9 or [^{18}F]FDR-Siglec-9. After PET imaging various tissues were collected for *ex vivo* measurements with a gamma counter. Inflamed tissues were further studied with the digital autoradiography and histological staining. The expression of luminal VAP-1 in inflamed tissues was also studied by means of immunohistochemical stainings.

Inflammation in different experimental settings were clearly visualized with [^{68}Ga]DOTA-Siglec-9 PET. The [^{18}F]FDR-Siglec-9 uptake in atherosclerotic mouse model and an acute sterile inflammation in a turpentine oil-induced rat model were comparable with [^{68}Ga]DOTA-Siglec-9. Anti-inflammatory therapy with VAP-1 inhibitor (LJP1586) reduced macrophages in atherosclerotic plaques in mice. The expression of luminal VAP-1 in inflamed tissue was verified with fluorescence-based immunohistochemistry.

In conclusion, [^{68}Ga]DOTA-Siglec-9 and [^{18}F]FDR-Siglec-9 are promising imaging agents for *in vivo* imaging of inflammation. [^{68}Ga]DOTA-Siglec-9 was able to detect inflammation already in its early stage. VAP-1 is a promising target for both anti-inflammatory therapy and molecular imaging of inflammation.

Key words: inflammation, positron emission tomography, VAP-1, Siglec-9

TIIVISTELMÄ

Helena Virtanen o.s. Ahtinen

VAP-1 MOLEKYYLI *IN VIVO* KUVANTAMISEN KOHTEENA – VALKOSOLUJEN KULKEUTUMINEN TULEHDUSPAIKALLE

Turun yliopisto, Lääketieteellinen tiedekunta, Kliininen fysiologia ja isotooppilääketiede, Lääketutkimuksen tohtoriohjelma, Valtakunnallinen PET keskus, Turku, Suomi

Tulehduksella on merkittävä rooli useissa sairauksissa, kuten reumataudeissa, sydän-ja verisuoni- sekä aineenvaihduntasairauksissa. VAP-1 on tartuntamolekyyli valkosolujen tarttuessa verisuonten pintasoluihin. Tulehduksen seurauksena VAP-1 molekyyli siirtyy solun sisäisistä säilytysjyväsistä verisuonen pinnalle. Valkosolu tarttuu verisuonen pinnalla olevaan VAP-1 molekyyliin ja siirtyy verenkierrosta tulehduspaikoille. Siglec-9 on eräs leukosyyttien pinnalla esiintyvä VAP-1:n vastinmolekyyli eli ligandi. Siglec-9:n aminohappojärjestys tunnetaan ja molekyyliä voidaan valmistaa synteettisesti sekä käyttää tulehdusperäisten sairauksien kuvantamiseen positroniemissiotomografialla (PET).

Tässä työssä arvioitiin radioleimatun Siglec-9 merkkiaineen käyttökelpoisuutta bakteerin aiheuttamassa tulehduksessa rotan luuimplanttimallissa, kaniinin nivelkalvon tulehduksessa, tärpätillä aiheutetun steriilin tulehduksen rottamallissa sekä valtimokovettumataudissa hiirimallissa. Osatöissä eläimet kuvattiin merkkiaineilla [^{68}Ga]DOTA-Siglec-9 tai [^{18}F]FDR-Siglec-9, jonka jälkeen eläimet lopetettiin. Lopetuksen jälkeen mielenkiintokudoksille tehtiin gammamittaus. Tulehtuneille kudoksille suoritettiin vielä herkempi autoradiografia-mittaus sekä histologiset värjäykset. VAP-1 molekyylin ilmentyminen verisuonten pinnalla tutkittiin immunohistokemiallisin menetelmin.

 [^{68}Ga]DOTA-Siglec-9 merkkiaineen kertymä tulehtuneessa kudoksessa pystyttiin havaitsemaan PET-kuvantamisen avulla. Steriilin tulehduksen rottamallissa sekä valtimokovettumataudissa hiirimallissa [^{18}F]FDR-Siglec-9:n kertymä kudoksiin oli samankaltainen [^{68}Ga]DOTA-Siglec-9:n merkkiaineen kanssa. Valtimokovettumataudissa kokeellisessa hiirimallissa makrofagien määrä väheni VAP-1-inhibiittorihoidon (LJP1586) aikana. Verisuonten sisäpinnan VAP-1 molekyylin ilmentyminen pystyttiin havaitsemaan fluoresenssiin perustuvilla immunohistokemiallisilla värjäyksillä.

[^{68}Ga]DOTA-Siglec-9 ja [^{18}F]FDR-Siglec-9 ovat lupaavia merkkiaineita tulehduksen PET-kuvantamiseen. [^{68}Ga]DOTA-Siglec-9 avulla pystyttiin osoittamaan tulehdus jo hyvin aikaisessa vaiheessa. VAP-1 molekyyli on lupaava kohde tulehduksen molekyylikuvantamiselle sekä tulehdusta vähentävälle lääkehoidolle.

Avainsanat: tulehdus, positroniemissiotomografia, VAP-1, Siglec-9

TABLE OF CONTENTS

ABBREVIATIONS

AOC	Copper-containing amine oxidase
APC	Antigen presenting cell
CD	Cluster of definition
CD99L2	CD99 antigen-like protein 2
COX	Cyclo-oxygenase
CRC	Colorectal cancer
CT	Computed tomography
DAMP	Damage associated molecular pattern
DOTA	1,4,7,10-tetraazacyclododecane-N,N′,N″,N‴-tetraacetic acid
ECT	Emission computed tomography
FDG	Fluorodeoxyglucose
FUO	Fever with undetermined origin
GDP	Guanosine 5'-diphosphate
GLUT	Glucose transporter
GlyCAM	Glycosylation-dependent cell adhesion molecule
GM-CSF	Granulocyte-macrophage colony-stimulating factor
GTP	Guanosine-5'-triphosphate
GTPase	An enzyme that can hydrolyze guanosine triphosphate
hAOC	Human copper containing amine oxidase
HMPAO	Hexamethylpropyleneamine oxime
ICAM	Intra cellular adhesion molecule
INF-α	Interferon alpha

iNOS	Inducible nitric oxide synthases
IBD	Inflammatory bowel disease
IFN-γ	Interferon gamma
IL	Interleukin
ILC	Innate lymphoid cell
JAM	Junctional adhesion molecule
LFA	Lymphocyte function-associated antigen
LPS	Lipopolysaccharides
LTi	Lymphoid tissue inducer
mAb	Monoclonal antibody
MadCAM	Mucosal vascular addressin cell adhesion molecule
MAC-1	Macrophage-1 antigen
MAO	Monoamine oxidase
M-CSF	Macrophage colony—stimulating factor
MCP	Monocyte chemoattractant protein
MHC	Major histocompatibility complex
MRI	Magnetic resonance imaging
mRNA	Messenger ribonucleic acid
NAD	Nicotinamide adenine dinucleotide
NETs	Neutrophil extracellular traps
NF-κB	Nuclear factor-κB
NK cell	Natural killer cell
NK-T cell	Natural killer T cell

PAMP	Pathogen associated molecular patterns
PECAM	Platelet endothelial cell adhesion molecule
PET	Positron emission tomography
PGE$_2$	Prostaglandin E2
PI3-kinase	Phosphoinositide 3-kinase
PMNL	Polymorphonuclear leukocytes
PSGL-1	P-selectin glycoprotein ligand-1
PRR	Pattern recognition receptors
RAGE	Receptor for advanced glycation endproducts
RA	Rheumatoid arthritis
Rac	Protein superfamily of small GTPases
RF	Rheumatoid factor
RGD	Amino acid sequence Arginine-Glycine-Aspartic acid
Rho	Protein superfamily of small GTPases
ROS	Reactive oxygen species
RRMS	Relapsing-Remitting Multiple Sclerosis
Siglec	Sialic acid-binding immunoglobulin-like lectin
SPECT	Single photon emission computed tomography
SSAO	Semicarbazide-sensitive amine oxidase
sVAP-1	Soluble vascular adhesion protein-1
TCR	T cell receptor
TEM	Transendothelial migration
TGF-β	Tumor growth factor beta

Th cell   T helper cell

TNFα   Tumor necrosis factor-α

TPQ   Topaquinone

VAP-1   Vascular adhesion protein-1

VCAM   Vascular cell adhesion molecule

VLA-4   Very late antigen-4

WBC   White blood cell

LIST OF ORIGINAL PUBLICATIONS

This thesis is based on the following original publications, which are referred to in the text by the Roman numerals I–V, and on some supplementary unpublished data.

I   Helena Ahtinen*, Julia Kulkova* Laura Lindholm, Erkki Eerola, Antti J. Hakanen, Niko Moritz, Mirva Söderström, Tiina Saanijoki, Sirpa Jalkanen, Anne Roivainen, Hannu T. Aro. ^{68}Ga-DOTA-Siglec-9 PET/CT imaging of peri-implant tissue responses and staphylococcal infections. EJNMMI Research 2014;4:45. *Equal contribution

II   Helena Virtanen, Anu Autio, Riikka Siitonen, Heidi Liljenbäck, Tiina Saanijoki, Petteri Lankinen, Jussi Mäkilä, Meeri Käkelä, Jarmo Teuho, Nina Savisto, Kimmo Jaakkola, Sirpa Jalkanen, Anne Roivainen. ^{68}Ga-DOTA-Siglec-9 – a new imaging tool to detect synovitis. Arthritis Research & Therapy 2015;17:308.

III   Xiang-Guo Li, Anu Autio, Helena Ahtinen, Kerttuli Helariutta, Heidi Liljenbäck, Sirpa Jalkanen, Anne Roivainen, Anu J. Airaksinen. Translating the concept of peptide labeling with 5-deoxy-5-[^{18}F]fluororibose into preclinical practice: ^{18}F-labeling of Siglec-9 peptide for PET imaging of inflammation. Chemical Communications 2013;49:3682-3684.

IV   Johanna M.U. Silvola*, Helena Virtanen*, Riikka Siitonen, Sanna Hellberg, Heidi Liljenbäck, Olli Metsälä, Mia Ståhle, Tiina Saanijoki, Meeri Käkelä, Harri Hakovirta, Seppo Ylä-Herttuala, Pekka Saukko, Matti Jauhiainen, Tibor Z. Veres, Sirpa Jalkanen, Juhani Knuuti, Antti Saraste, Anne Roivainen. Leukocyte trafficking-associated vascular adhesion protein 1 is expressed and functionally active in atherosclerotic plaques. Scientific Reports 2016;6:35089. *Equal contribution

V   Helena Virtanen, Johanna M.U. Silvola, Anu Autio, Xiang-Guo Li, Heidi Liljenbäck, Sanna Hellberg, Riikka Siitonen, Mia Ståhle, Meeri Käkelä, Anu J. Airaksinen, Kerttuli Helariutta, Tuula Tolvanen, Tibor Z. Veres, Antti Saraste, Juhani Knuuti, Sirpa Jalkanen, Anne Roivainen. Comparison of ^{68}Ga-DOTA-Siglec-9 and ^{18}F-Fluorodeoxyribose-Siglec-9: Inflammation Imaging and Radiation Dosimetry. Manuscript submitted for publication.

The original publications have been reproduced with the permission of the copyright holders.

1. INTRODUCTION

The classic signs of inflammation are pain, redness, swelling and heat that usually occur as a response to physical injury, infection or a local immune response. Infection acquires an infectious agent that invades and multiplies in the body and may lead to clinical symptoms as the immune response of the host is activated. In general, inflammation is a term for the local accumulation of fluid, plasma proteins and white blood cells (Murphy Kenneth et al 2008). Inflammation is related to many common diseases, such as atherosclerosis, diabetes and rheumatoid arthritis (RA). Inflammation can be divided into acute and chronic states. Acute inflammation occurs rapidly within a few hours after injury, resulting in elimination of the infectious agent. Chronic inflammation occurs later on when the inflammation is prolonged. Inflammation possesses special characteristics, which can be identified in the different states of inflammation. Chronic inflammation behind autoimmune diseases and chronic infections are rather well known. Much less is known about systemic chronic inflammation, which causes malfunction in tissue and changes in homeostasis between different physiological functions (Medzhitov 2008).

Activation of the endothelium enables many pro-inflammatory processes, such as leukocyte extravasation. Transendothelial migration (TEM) of leukocytes is tightly controlled and requires adhesion molecules. In this process, circulating leukocytes must first adhere to the luminal surface on the endothelium. Leukocyte extravasation cascade includes many phases, such as rolling, adhesion and transmigration, which are the main steps of TEM. Activated endothelium expresses adhesion molecules that mediate the binding of one cell to another cell or to extracellular matrix proteins and enable the leukocytes' extravasation and accumulation into the site of inflammation. Adhesion molecules are important in the operation of the immune system and uncontrolled or excessive TEM is related to many inflammatory diseases (Vestweber 2015).

Many radiopharmaceuticals have been developed for PET imaging of inflammation, targeting different biomarkers from macrophages to angiogenesis. In inflammation, locally changed conditions, such as enhanced blood flow, enhanced vascular permeability and influx of white blood cells, promote the accumulation of any imaging agents at the site of inflammation. [^{18}F]FDG (2-deoxy-2-[^{18}F]-fluoro-D-glucose) is the most common PET imaging tracer and widely used especially in oncology (tumor detection, staging and therapy evaluation). [^{18}F]FDG is also feasible in infection imaging for example in

sarcoidosis, peripheral bone osteomyelitis and fever with undetermined origin (FUO) (Jamar *et al.* 2013). Because the uptake of [^{18}F]FDG is based on increased glucose uptake, the major disadvantage of [^{18}F]FDG PET is the possibility of false-positive results, for example, it may not be able to discriminate tumor from inflammation (Wu *et al.* 2013). The discrimination of infection from aseptic loosening of prosthesis is also difficult (Love *et al.* 2005). In addition, the high physiological accumulation of [^{18}F]FDG in the heart and brain makes it difficult to detect inflammatory foci close to these organs. Development of new inflammation imaging agents is challenging due to their unspecific uptake (Wu *et al.* 2013).

Vascular adhesion protein-1 (VAP-1) is an endothelial adhesion molecule involved in leukocyte trafficking cascades from blood circulation to the sites of inflammation. It is a sialylated 180 kDa homodimeric glycoprotein, which is, upon inflammation, rapidly translocated from the intracellular storage granules to the endothelial cell surface. In addition to being an adhesion molecule, VAP-1 has also enzymatic activity. Structurally VAP-1 is a copper-containing semicarbazide-sensitive amine oxidase (SSAO) that deaminates primary amines producing hydrogen peroxide, aldehyde and ammonia. VAP-1/SSAO activity also enhances the production of other adhesion molecules, such as E- and P-selectins, ICAM-1 and VCAM-1. Although leukocytes can bind to endothelium via VAP-1, their counter-receptors were for a long time unknown. It was recently discovered that sialic acid binding immunoglobulin-like lectin 9 and 10 (Siglec-9 and Siglec-10) are leukocyte ligands of VAP-1 (Kivi *et al.* 2009; Aalto *et al.* 2011). In addition, ^{68}Ga-labeled Siglec-9 motif containing peptide can be used as a PET tracer for *in vivo* imaging of inflammation and cancer (Aalto *et al.* 2011).

For this study, the novel VAP-1 targeting PET tracer, radiolabeled Siglec-9, is investigated for its potential to detect inflammation in various diseases. This research project consists of five subprojects in which the feasibility of Siglec-9 in *in vivo* PET imaging is explored in experimental inflammatory animal models.

2. REVIEW OF THE LITERATURE

2.1 Inflammation

In the 1st century, the Roman medical encyclopedist Aulus Cornelius Celsus defined the four cardinal signs of inflammation as follows: *rubor et tumor cum calore et dolore* (redness and swelling with heat and pain). *Functio laesa* (disturbance of function) was added by Rudolf Virchow in 1858 as the fifth cardinal sign of inflammation. Redness, swelling and pain are local symptoms of inflammation, whereas fever is sign of systemic response. Today, it is known that inflammation occurs in different forms and modalities. The survival of all organisms requires a capability to eliminate foreign invaders, such as infectious agents, and damaged tissues. The pathogenesis of inflammation is a complex biological process and it involves many different cell types and co-operation with inducers, sensors, mediators and target tissues, which results in the elimination of the initial cause of cell injury, as well as the initiation of the repair process. Exogenous inducers can be divided into microbial and non-microbial types. Pathogen-associated molecular patterns (PAMPs) are derived from micro-organisms and damage associated molecular patterns (DAMPs) from injured tissue cells. Microbial inducers include PAMPs and virulence factors. Exogenous non-microbial inducers include allergens, irritants, foreign bodies and toxic components. Signals produced by stressed, damaged or malfunctioned tissues are called endogenous signals of inflammation (Medzhitov 2008). These signals stimulate the cells of the innate immune system, which leads to the secretion of cytokines and other pro-inflammatory mediators. The mediators activate the microvasculature near the inflammation site (Vestweber 2015). In normal conditions, inflammation is a controlled process and self-limited when the injurious stimuli are eliminated. If the stimuli are not eliminated rapidly, it may result in chronic inflammation and the components of inflammatory response and subsequent repair process may be harmful. A beneficial inflammatory response can become dominant and cause a very strong reaction (when the infection is severe), or it can be prolonged (when the causal agent resists eradication) or inappropriate (when it is directed against self-antigens in autoimmune diseases or allergy disorders) (Kumar, Abbas and Aster 2013).

2.1.1 Acute inflammation

Inflammation is divided into acute and chronic states (Figure 1.). The acute inflammation is rapid, lasting from a few minutes to a few days. It is characterized by 1) vasodilatation and increased blood flow, 2) increased vascular permeability (edema) and 3) infiltration of polymorhonuclear leukocytes (PMNL) (Roivainen, Jalkanen and Nanni 2012). Acute inflammation is comprised of initiation and resolution phases. Common characteristics of initiation phase are edema as a result of increased blood flow and permeability of microvasculature, which is partly mediated by lipid mediators and other vasoactive products. Subsequently, polymorphonuclear neutrophils (PMN) migrate to the site of inflammation. PMN extravasation to the site of inflammation requires interactions between adhesion receptors on the endothelium (Sansbury and Spite 2016).
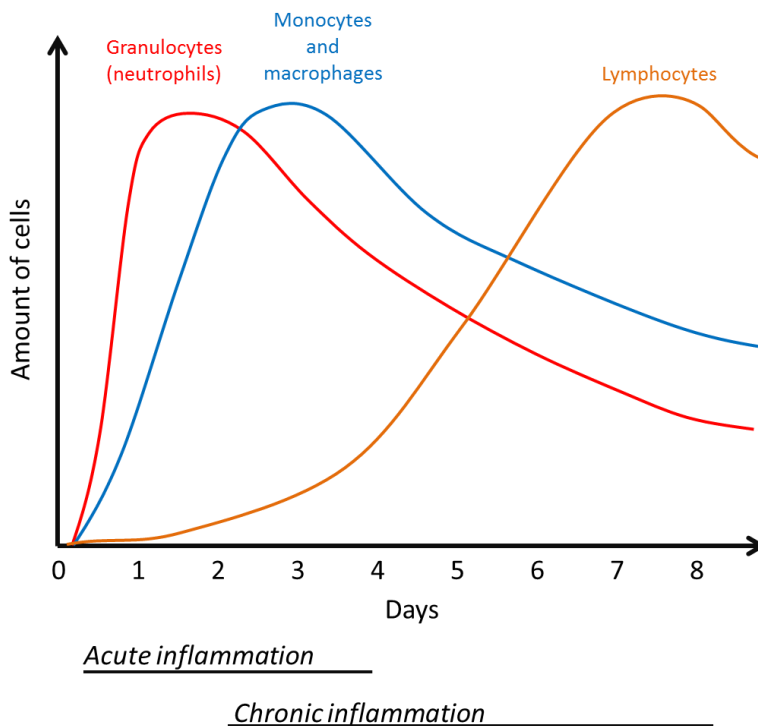

Figure 1. Inflammation is divided into acute and chronic states and it requires co-operation between granulocytes, monocytes/macrophages and lymphocytes.

2.1.2 Chronic inflammation

Chronic inflammation denotes prolonged inflammation with simultaneously proceeding inflammation, infiltration of mononuclear cells, tissue destruction and repair, including vascular proliferation (angiogenesis) and fibrosis. Both acute and chronic inflammatory responses are dependent on the leukocyte trafficking across the endothelium (Luster, Alon and von Andrian 2005).

2.1.3 Inflammation in osteomyelitis

Osteomyelitis is a destructive process of the bone because of an infection with an extensive inflammatory component. The infection can involve single or multiple regions, such as marrow, cortex, periosteum and surrounding tissue (Lew and Waldvogel 2004). The development of osteomyelitis can be divided into three major phases: 1) microbial invasion and biofilm proliferation, 2) immune response to the bacterial biofilm, and 3) impact of bacterial invasion on bone tissue components (Beck-Broichsitter, Smeets and Heiland 2015). Osteomyelitis can occur at any age. Trauma, bone surgery or joint replacement allow free entry of infectious agents from the contaminated source to the bone (Lew and Waldvogel 2004).

Biomaterial-related infections are a common cause of implant failure in joint replacements. Biomaterials include metal, polymer or ceramic. Approximately two thirds of the orthopedic implant infections are caused by staphylococcal bacteria (Neut *et al.* 2007). *S. aureus* and *S. epidermidis* are the most common coagulase-positive and coagulase-negative staphylococcal species, respectively. The clinical picture of infections caused by *S. epidermidis* is usually subtle and non-specific. The clinical course of such infections is also often more sub-acute than chronic and the classical signs of infection are missing, whereas *S. aureus* is known as a cause of classical pyogenic infection with enzyme-mediated bone destruction and new bone formation (Lew and Waldvogel 1997; von Eiff, Peters and Heilmann 2002). *S. aureus* is more frequently found in hematogenous and posttraumatic osteomyelitis, whereas *S. epidermidis* is the leading nosocomial pathogen of biomaterial-related bone infections (Lew and Waldvogel 2004). The pathogenesis of polymer-associated infections due to *S. epidermidis* is characterized by the bacterial ability to colonize the polymer surface and to form a thick, multilayer biofilm. *S. epidermidis* is normally found on human skin or mucous membranes where it can easily contaminate laboratory devices. Biofilm formation starts when bacteria rapidly adhere to the polymer material. In the

accumulation phase, the bacteria proliferate and form multilayered cell clusters on the polymer surface (von Eiff, Peters and Heilmann 2002).

S. epidermidis infection is challenging to detect and treat because it is clinically indolent and also due to its capability to produce biofilm, which protects the pathogen against natural host defense and antibiotics. This also sets challenges for diagnostic imaging because of the limited inflammatory host response against the pathogen (Lankinen *et al.* 2012). Moreover, the differentiation between aseptic loosening and infection in joint replacements is a major diagnostic challenge as there is no single routine test that can recognize an infection with sufficiently high diagnostic accuracy. Often the signs and symptoms, expect pain, are lacking which makes it difficult to find the correct therapeutic approach (Palestro 2015).

The first fighters against the bacterial biofilm are the PMNLs. The maturation state of the biofilm affects the effectiveness of the immune response. An immature biofilm is an easier target for PMNLs (Günther *et al.* 2009). The biofilm also leads to an activation of monocytes and T cells, resulting in local increase of pro-inflammatory cytokines. The continuous release of inflammatory mediators will lead to osteolytic and tissue damaging processes. Various inflammatory factors contribute to necrosis in osteomyelitis. The inflammatory process also compresses and obliterates vascular channels and causes ischemia, which increases necrosis of the bone. This leads to failed medical treatment and impaired response of the inflammatory cells, which supports the relevance of early detection of infection (Lew and Waldvogel 2004).

2.1.4 Inflammation in rheumatoid arthritis

RA is a common chronic autoimmune disease, which includes both genetic and environmental factors (McInnes and Schett 2011). It is a systemic inflammatory disease that can affect many tissues and organs as well as synovial joint (Cojocaru *et al.* 2010). The synovial membrane is normally 1-2 cell layers thick but in RA, synovium consists of multiple cell layers, due to cellular hyperproliferation and infiltration of immune cells (macrophages, T cells, B cells). The hallmark of RA is inflamed synovial tissue (synovitis) (Cascão *et al.* 2010). Synovial hyperplasia leads to pannus formation and oxygen deprivation, which induce angiogenesis (Konisti, Kiriakidis and Paleolog 2012). Many inflammatory chemokines, which are needed for transendothelial migration, are involved in synovial neovascularization. The rheumatoid synovial tissue is rich of neovessels, which also increase the area of the vessel wall/endothelium in the

synovium and may increase the transmigration of the leukocytes and enhance the progression of RA (Szekanecz *et al.* 2009). Hyperplastic synovium results in structural damages, such as cartilage destruction and impairs joint movement. If, in spite of disease-modifying anti-rheumatic treatment, synovial inflammation and pannus formation persist, it may eventually lead also to bone erosions (Schett and Gravallese 2012).

The functional role of T cells in RA is not fully understood. T cells are found abundantly in the inflamed synovium but direct targeting by cyclosporine or T cell depleting therapy has shown limited efficacy (Panayi 2006). Type 1 helper T cells (Th1) and especially type 17 helper T cells (Th17) have been in the focus in RA. The Th17 subset produces interleukins 17A, 17B, 21, 22 and tumor necrosis factor α (TNFα). The imbalance between regulatory T cells and inflammatory Th17 cells is suggested to be one critical factor in RA (Komatsu *et al.* 2013). B cells act as antigen presenting cells and are capable of autoantibody production. In synovial membrane, plasma cells contain rheumatoid factor (RF), which acts as a self-perpetuating stimulus for RA. RF also binds to Fc-receptor on the macrophages and enhances the secretion of pro-inflammatory cytokines (McInnes and Schett 2011; Burmester, Feist and Dörner 2013).

Macrophages are the key effectors in RA; they produce cytokines, which promote inflammation by recruiting other immune cells, T cell polarization and fibroblast activation. In the inflamed joint, macrophages are the main TNF-producing cells and the abundance and activation of macrophages correlates with the disease severity (Udalova, Mantovani and Feldmann 2016). Macrophages promote inflammation also by producing reactive oxygen species (ROS), nitrix oxide (NO) intermediates and matrix-degrading enzymes as well as participating antigen presentation (McInnes and Schett 2007).

2.1.5 Inflammation in atherosclerosis

Cardiovascular diseases are the leading cause of deaths in developed countries. Atherosclerosis is a common cardiovascular disease and can lead to coronary heart disease, myocardial infarction and vertebral hemorrhage (Packard, Lichtman and Libby 2009). Atherosclerosis is a chronic inflammatory disease that is characterized by the accumulation of lipids in arterial wall. Development of atherosclerotic lesions also includes infiltration of immune cells, such as macrophages, T cells and mast cells, and the formation of fibrous cap by smooth muscle cells. Early atherosclerotic lesions consist of sub-endothelial deposition of lipids, macrophage foam cells and T cells. The more advanced lesions consist

of apoptotic and necrotic cells, cell debris and cholesterol crystals forming the necrotic core covered with the fibrous cap. Plaque growth narrows the lumen and promotes ischemia in the surrounding tissue. When the surface of the plaque ruptures it causes platelet aggregation, humoral coagulation and thrombus formation, which can have life-threatening consequences, such as myocardial infarction or cerebral infarction (Hansson and Hermansson 2011).

In atherosclerosis, macrophages have a central role in the disease progression. The number of macrophages correlates with the plaque progression and plaque rupture. Monocytes differentiate into macrophages in arterial intima under the influence of macrophage-colony stimulating factor (M-CSF). It induces the expression of scavenger receptors and pattern-recognition receptor expression on the macrophage surface. They phagocytose the modified lipoproteins and apoptotic structures via receptor-mediated endocytosis, leading to lysosomal degradation. Scavenger receptors also involve the foam cell formation. Granulocyte-macrophage colony stimulating factor (GM-CSF) increases the volume of the macrophages and enhances the inflammatory reaction in atherosclerotic lesions. The influence of growth factors and cytokines causes the migration of the vascular smooth muscle cells from the media to the intima. Infiltration of macrophages and T cells and proliferation of cognitive tissue leads to vascular remodeling (Woollard and Geissmann 2010; Wang *et al.* 2016).

2.2 Immune response

Immune response is divided into innate immunity and adaptive immunity. Innate immunity is the first line defense against invading pathogens. In the initial step of immune response, neutrophils are the main cell type. Innate immune system recognizes pathogens via pattern recognition receptors (PRR), which are expressed on the cellular surface of innate immune cells or distinct intracellular compartments. When the innate immune system is activated it leads to the production of cytokines and chemokines that further enhance immune response. Monocytes, which rapidly differentiate into macrophages, are the next fighters in inflammation. If the pathogen cannot be destroyed via innate immune response, the more sophisticated, adaptive immune system is activated. Adaptive immune response is lymphocyte specific response against a particular antigen and provides long lasting protection. Signaling molecules, such as cytokines and complement fragments, are important factors in leukocyte trafficking to the site of inflammation (Chaplin 2010).

Immune system is formed of a set of stem-cell derived lineages. The pluripotent cell differentiates into myeloid stem cells or common lymphoid progenitors. These cells differentiate further. Myeloid stem cells differentiate into different forms of granulocytes, megakaryocytes, platelets and erythrocytes. The granulocyte lineage consists of neutrophils, eosinophils, basophils, mast cells and monocytes, which all have a remarkable role in immune system. The common lymphoid progenitor differentiates into mature lymphocytes, such as B cells, T cells, natural killer cells (NK cells) and natural killer T cells (NKT-cells). An intact immune response includes many cellular elements and participation of many subsets of leukocytes. Discrimination between different types of leukocyte subtypes can be made based on morphology and by differentiation of cell surface antigens. These antigens can be detected with specific monoclonal antibodies and are called cluster of differentiation (CD) antigens. CD antigens are cell surface markers, which are expressed on leukocytes and reveal cell lineage, developmental stage and functional subsets. Over 350 defined CD antigens are known (Chaplin 2010).

2.2.1 Polymorphonuclear leukocytes

Neutrophils are the most abundant immune cell type and they form the first line defense of the innate immune response. Tissue-resident macrophages and other sentinel cells secrete cytokines and other chemoattractants that guide neutrophils to migrate into the site of inflammation, where they recognize the pathogen and destroy it with phagocytosis or degranulation (Sadik, Kim and Luster 2011). Excessive neutrophil degranulation is a common feature of many inflammatory disorders, for example, acute lung injury, RA and septic shock (Lacy 2006). Neutrophils also release web-like extracellular structures that are called neutrophil extracellular traps (NETs). This structure traps, neutralizes and kills variety microbes (Branzk and Papayannopoulos 2013). In response to infection or inflammation neutrophils are released from the blood marrow, which is a rapid way to increase circulating neutrophils. Neutrophils release pro-inflammatory factors and several cytokines and actively regulate inflammatory response (Rosales *et al.* 2016). Other PMNL are eosinophils and basophils/mast cells that have essential function in allergic inflammation (Parkin and Cohen 2001).

2.2.2 Natural killer cells

Natural killer (NK) cells are a subset of cytotoxic innate lymphoid cells (ILCs) and effector cells of the innate immune system. ILCs are a group of innate lymphoid cells that includes NK cells, lymphoid tissue inducer (LTi) cells and

other non-T or non-B cells that produce cytokines, such as interleukin-5 (IL-5), IL-13, IL-17 and IL-22. ILCs and secreted cytokines initiate immune responses against pathogens. NK cells limit spread of tumors and microbial infections. NK cells activity is tightly regulated by multiple cell surface receptors which have activating and inhibiting effects. NK cells secrete cytokines, such as interferon-γ (IFNγ), which are involved in the recruitment of adaptive immunity. NK cells have a capability to recognize and destroy stressed cells (tumor cells, infected cells, injured cells) (Vivier *et al.* 2012). Natural killer T (NKT) cells can be roughly described as a T cell lineage which expresses NK lineage markers. Mature NKT cells are capable of producing massive amounts of IFNγ, IL-4 and other key Th2 cytokines (Balato, Unutmaz and Gaspari 2009).

2.2.3 Monocytes

Monocytes are differentiated from hematopoietic stem cells. In inflammation, monocytes migrate into the sites of inflammation and differentiate into macrophages and dendritic cells. Differentiation depends on the tissue environment, such as signaling molecules, and the type of inflammation. Macrophages are involved in phagocytosis of tissue debris or foreign materials, and they regulate steady state defense and tissue healing. Macrophages also produce inflammatory cytokines, which can enhance the progression of the disease (Dutta and Nahrendorf 2014).

In *in vitro* settings, the Th1-derived pro-inflammatory IFNγ and Th2-derived anti-inflammatory IL-4 and -13 have lead the original concept of analogous M1 and M2 macrophages. IFNγ is the main cytokine that is related to the M1 macrophage production and IL-1, IL-4 and IL-13 are related to the M2 activation. However, this classification is only rarely found in *in vivo* settings and macrophage subpopulations divide into wide heterogeneity, where the M1 and M2 stated macrophages represent extremes of the polarization states (Mantovani, Garlanda and Locati 2009; Martinez and Gordon 2014). The pro-inflammatory M1 macrophages are strongly involved in the resistance to intracellular pathogens and to tumors in the context of Th1 response. M1 macrophages promote inflammation with high production of IL-1b, IL-6 and IL-12 and enhanced inducible nitric oxide synthase (iNOS) (Murray *et al.* 2014; Xue *et al.* 2014). M2 macrophages are predominantly involved in the resistance of parasites, promote tumor growth and invasiveness, have immune regulatory effects, participate in healing process (tissue repair and remodeling), including fibrosis, and are involved in angiogenesis. M2 macrophages secrete anti-

inflammatory cytokines, such as TGF-β and IL-1 receptor antagonist and IL-10 (Mantovani, Sica, and Locati 2005; Gordon and Martinez 2010).

2.2.4 Lymphocytes

Immature lymphocytes develop in primary lymphoid organs, which include thymus (T cells) and bone marrow (B cells and hematopoiesis). These lymphocytes develop further upon antigen exposure in secondary lymphoid organs, such as spleen, lymph nodes, tonsils, appendix and Peyer's patches. Dendritic cells are known as antigen presenting cells (APC) and are efficient stimulators to recruit B and T lymphocytes. The precursor B cells recognize the antigen via B cell receptors, which recognize a primary antigen and recruit antibody secreting cells. These antibody-secreting cells are called effector B cells and are responsible for humoral immunity. Every B cell produces a single type of antibody.

T cells are required for cellular immunity. For T cell recruitment, the antigens must be processed to peptide fragments. APCs take up the antigen via phagocytosis or pinocytosis. T cell receptors (TCR) recognize the fragments of antigens, which are bound to the major histocompatibility complex I or II (MHC I and MHC II) (Chaplin 2010). MHC I recruits cytotoxic $CD8^+$ cells and MHC II $CD4^+$ T helper (Th) cells. CD8 T cells are designed to become cytotoxic T cells. CD4 T cells can differentiate into various types of effector T cells after initial activation by an antigen. Two major cell types of CD4 effector cells are Th1 and Th2 cells. Th cells have a crucial role in the development of adaptive immunity. Th cells have regulatory and effector functions in the activation of cytotoxic T cells and also in the development of antigen specific B cell memory, which occurs in several steps and checkpoints. B cells can proliferate into short-lived antibody producing plasma cells, memory B cells or long-lived plasma cells that contribute to the serological memory (Kurosaki, Kometani and Ise 2015).

2.3 Leukocyte extravasation

Transendothelial migration (TEM) is a well-controlled process which requires adhesion molecules (Table 1). Adhesion molecules are surface bound molecules, which facilitate processes requiring a close contact of cells. Unbalanced, excessive TEM is characterized in several chronic inflammatory diseases, for example atherosclerosis, RA and asthma as well as in progressive cancer. Association with cytoplasmic proteins and cytoskeletal components causes cytoskeletal reorganization, which allows cells to undergo direct movement

(Parkin and Cohen 2001; Heemskerk, van Rijssel and van Buul 2014). Leukocyte extravasation includes several steps, which are rolling (tethering, slow rolling), adhesion (full arrest, firm adhesion), crawling and transmigration. In the leukocyte adhesion cascade each step is essential to achieve the next (Heemskerk, van Rijssel and van Buul 2014; Nourshargh and Alon 2014).
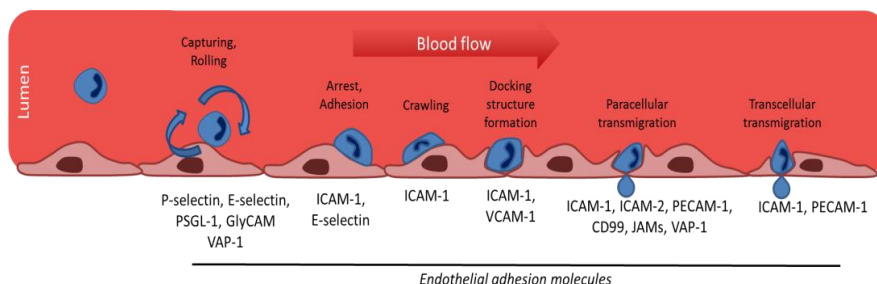

Figure 2. Characteristics of the leukocyte extravasation cascade. Leukocyte migration utilizes adhesion molecules that enable leukocytes to interact with endothelial cells.

The extravasation cascade begins with leukocyte tethering and rolling on the endothelium. P- and E-selectins on the endothelium interact with their leukocyte counterparts L-selectins and P-selectin glycoprotein-1 (PSGL-1). Weibel-Palade bodies are granules in the endothelial cells that contains P-selectin. Endothelial activation leads to a rapid P-selectin translocation on the endothelial cell surface. E-selectin is not found in the Weibel-Palade bodies but it is expressed on the endothelium under inflammatory stimuli. Up-regulation of both P-and E-selectins requires the involvement of small Rho-GTPases; RhoA, RhoB and Rac (Cernuda-Morollón and Ridley 2006). All Rho GTPases bind to guanosine-5'-triphosphate (GTP) and most of them exhibit GTPase activity between an inactive guanosine 5′-diphosphate (GDP) bound and active GTP-bound form. In GTP-bound form, Rho GTPases interact with their downstream effectors such as regulators in actin polymerization, and other proteins which have adaptor functions (Mizuno-Yamasaki, Rivera-Molina and Novick 2012). Subsequently, the velocity of the rolling is reduced via the adhesive interactions of selectins and integrins resulting in the slow rolling step and finally arresting the cells firmly on the endothelium. The subsequent step is crawling, during which the leukocytes are seeking for an appropriate place for transmigration. Leukocyte crawling is mediated by leukocyte integrins, such as very late antigen-4 (VLA-4), lymphocyte function associated antigen-1 (LFA-1) or macrophage-1 antigen (MAC-1), which interact with their endothelial ligands, including vascular cell

adhesion molecule-1 (VCAM-1) and intercellular adhesion molecules 1 and 2 (ICAM-1, ICAM-2). Transmigration is the final step and it is mediated via several adhesion receptors, such as integrins, junctional adhesion molecules (JAMs), platelet endothelial adhesion molecule-1 (PECAM-1) or CD99. Cytokines and chemokines can modulate the different steps of extravasation cascade (Chavakis *et al.* 2003; Phillipson and Kubes 2011; Hajishengallis and Chavakis 2013). Characteristics of the leukocyte adhesion cascade are presented in Figure 2.

Table 1. Adhesion molecules involved in the leukocyte extravasation cascade.

Endothelial adhesion receptor	Role	Leukocyte ligand	Ref.
P-selectin E-selectin VAP-1 PSGL1, GlyCAM	Rolling	PSGL1 PSGL1, ESL1, CD44 SIGLEC-9, SIGLEC-10 L-selectin	(Vestweber and Blanks 1999; Salmi and Jalkanen 2001; Kivi *et al.* 2009; Aalto *et al.* 2011; McEver 2015)
ICAM-1 VCAM-1	Adhesion	LFA1 VLA4	(Marlin and Springer 1987; Carlos and Harlan 1994; Barreiro *et al.* 2002)
ICAM-1, ICAM-2	Crawling	MAC1	(Marlin and Springer 1987; Carlos and Harlan 1994; Barreiro *et al.* 2002; Halai *et al.* 2014)
ICAM-1, ICAM-2 VCAM-1 CD99 PECAM1 JAMA JAMB JAMC CD99L2 VAP-1	Transmigration	LFA1, MAC1 VLA4 CD99 PECAM1 LFA1 VLA4 MAC1 Unknown SIGLEC-9, SIGLEC-10	(Marlin and Springer 1987; Carlos and Harlan 1994; Schenkel *et al.* 2002; Barreiro *et al.* 2002; Muller 2003; Aurrand-Lions *et al.* 2005; Nourshargh, Krombach and Dejana 2006; Woodfin *et al.* 2007; Dufour *et al.* 2008; Kivi *et al.* 2009; Aalto *et al.* 2011; Kolaczkowska and Kubes 2013; Halai *et al.* 2014; Watson *et al.* 2015)

2.3.1 VAP-1

Ectoenzymes are a unique class of cell surface enzymes, which are involved in leukocyte trafficking. Ectoenzymes are divided into the following major classes: oxidases, nicotinamide adenine dinucleotide (NAD) metabolizing enzymes, nucleotidases and related enzymes, peptidases and proteases. One of the best-characterized ectoenzyme is human primary amine oxidase (hAOC3), which is also known as vascular adhesion protein-1 (VAP-1) (Salmi and Jalkanen 2014).

VAP-1 was first discovered in inflamed synovial membranes in the 1990s by Jalkanen and Salmi. First, monoclonal antibodies (mAbs) were produced against purified synovial vessels from rheumatoid arthritis patients. One mAb (1B2) reacted with the synovial vessels and this antigen was named VAP-1 (Salmi and Jalkanen 1992). VAP-1 is not expressed at synovial endothelial cells only. It is also detected in high endothelial cells of lymphatic organs, sinusoidal endothelial cells in liver and small-caliber venules in many other tissues besides synovium (Salmi, Kalimo and Jalkanen 1993; Salmi and Jalkanen 2001). VAP-1 plays a role in several diseases, such as arthritis, multiple sclerosis, diabetes and atherosclerosis by participating to the immune cell trafficking to sites of inflammation (Jaakkola *et al.* 2000; Merinen *et al.* 2005; Airas *et al.* 2006).

VAP-1 differs from other adhesion molecules. In normal conditions, VAP-1 is stored in intracellular granules. These granules are distinct from Weibel-Palade bodies vs. P-selectin. During inflammation, VAP-1 is translocated onto the luminal surface of vessels only at sites of inflammation. Isolated populations of lymphocytes, such as NK cells and cytotoxic CD8+ cells, have shown VAP-1 dependent adhesion to vasculature (Salmi and Jalkanen 2001). Granulocyte migration is also VAP-1 mediated. Recently, new leukocyte ligands for VAP-1 have been found; Siglec-10 on monocytes, B cells and eosinophils and Siglec-9 on monocytes and granulocytes. Siglec-9 expression on the leukocyte surface is enhanced after inflammatory stimuli. TNFα and LPS significantly increase the upregulation of Siglec-9 and promote leukocyte trafficking (Salmi and Jalkanen 2001; Kivi *et al.* 2009; Aalto *et al.* 2011). Regarding metabolism, VAP-1 has insulin-like effects, which are mediated via PI3-kinase and enhanced via SSAO related hydrogen peroxide (H_2O_2) production (Enrique-Tarancón *et al.* 2000).

2.3.2 Structure of VAP-1

VAP-1 is an endothelial transmembrane molecule with a single transmembrane and a large extracellular domain. It is a heavily sialylated homodimeric type 2 glycoprotein. The VAP-1 structure consists of two identical monomeric subunits of 90 kDa and a short cytoplasmic tail. VAP-1 shares significant sequence identity with enzymes called semicarbazide-sensitive amine oxidases (SSAOs). VAP-1 differs from monoamine oxidases A and B (MAO-A, MAO-B) in terms of their amino acid sequence, subcellular localization, cofactors, substrates, inhibitor specificity and physiological function (Jalkanen and Salmi 2001).

In humans, four sources of SSAO has been identified which are copper containing amine oxidases (AOC1-3) and lysyl oxidase. VAP-1 (AOC3, EC1.4.3.6) is the most important source of primary amine oxidase in human serum. Human AOC3 gene is located on chromosome 17 (17q21.31). AOCs are copper and quinone-dependent enzymes that catalyze the oxidative deamination of exogenous (allylamine and benzylamine) and endogenous (methylamine and aminoacetone) primary amines producing end-products, such as aldehydes, hydrogen peroxide and ammonia. The general reaction of SSAO enzyme is $R\text{-}CH_2\text{-}NH_2 + O_2 \rightarrow R\text{-}CHO + H_2O_2 + NH_3$. SSAOs have a topa-quinone (TPQ) at the catalytic center. TPQ is a modified tyrosine residue and it is required for the enzymatic activation of many amine oxidases. The enzymatic reaction of VAP-1 involves reduction of primary amines with formation of transient Schiff base via TPQ. A mutation in this TPQ's tyrosine residue loses the oxidative function of SSAO (Koskinen *et al.* 2004; Noonan *et al.* 2013; Salmi and Jalkanen 2014). The end-products of primary amines also act as signaling molecules and promote the leukocyte adhesion cascade. H_2O_2 is a powerful redox-signaling molecule. VAP-1 generated H_2O_2 induces other adhesion molecules, such as P-and E-selectins, ICAM-1, VCAM-1, MadCAM-1 and chemotactic substances (IL-8, MCP), and activates transcription factors, such as (NF-κB and p53) (Jalkanen *et al.* 2007; Lalor *et al.* 2007; Solé *et al.* 2008; Liaskou *et al.* 2011). It has been shown that VAP-1 plays an important role in granulocyte extravasation *in vivo* (Tohka *et al.* 2001). Semicarbazide, hydroxylamine and other carbonyl-reactive compounds inhibit the activity of SSAOs (Jalkanen and Salmi 2001).

2.3.3 Soluble VAP-1

Besides the transmembrane form, VAP-1 also exists in a soluble form in plasma (sVAP-1) and it is partly regulated by changes in insulin level. sVAP-1 level is elevated in several inflammatory diseases (Kurkijärvi *et al.* 1998, 2000). The

concentration of sVAP-1 in healthy human plasma is approximately 80 ng/ml (Kurkijärvi *et al.* 1998). VAP-1 is expressed on blood vessels and it is suggested that sVAP-1 is generated through a proteolytic cleavage of the membrane-bound protein by metalloproteinase (Stolen *et al.* 2004).
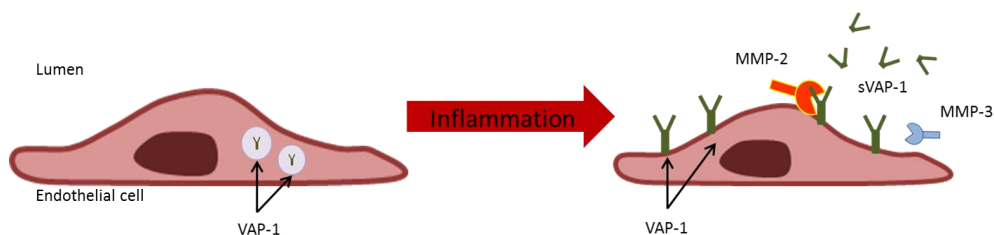

Figure 3. VAP-1 is upregulated on the endothelial cell surface in inflammation. Soluble VAP-1 is generated via proteolytic cleavage of membrane bound VAP-1

Inflammatory liver disease (Kurkijärvi *et al.* 1998) and diabetes (Salmi *et al.* 2002) are examples of diseases in which raised sVAP-1 concentrations have been observed. The concentration varied between 140 ± 61 ng/ml for inflammatory liver disease (Kurkijärvi *et al.* 1998) and 116.7 ± 43.3 ng/ml for Type-I diabetes (Salmi *et al.* 2002). In contrast, in colorectal cancer (CRC) patients, circulating sVAP-1 levels in plasma were lower as compared to the controls. Additionally, sVAP-1 correlated negatively with lymph node and hepatic metastases in CRC patients. Lymph node metastases are the most important predictors in non-stage IV colorectal cancer, suggesting that sVAP-1 could be a good predictor of over-all prognosis of CRC patients (Toiyama *et al.* 2009; Li *et al.* 2014c; Ward *et al.* 2016). However, a 10-year cohort study indicated increased sVAP-1 levels in patients with Type-2 diabetes and CRC. The same study also demonstrated that sVAP can independently predict 10-year all-cause mortality, cardiovascular mortality and cancer mortality (Li *et al.* 2011). Increased sVAP-1 levels have also been found in patients with atopic eczema (Madej *et al.* 2006) and relapsing-remitting multiple sclerosis (RRMS) (Airas *et al.* 2006), and it also correlated directly with cardiovascular risk factors such intima-media thickness and carotid plaques (Aalto *et al.* 2012).

2.3.4 Inhibition of VAP-1

VAP-1 is a unique target molecule for anti-inflammatory therapy in many acute and chronic inflammatory conditions (Dunkel *et al.* 2011). Blocking the

functional activity of VAP-1 with antibodies, small-molecule enzyme inhibitors and use of AOC3 gene-deficient mice have given tools to investigate leukocyte trafficking and clarify the role of VAP-1 during this process (Salmi and Jalkanen 2012). It is suggested that leukocytes first make VAP-1-dependent contacts with endothelium using epitopes, which can be blocked with anti-VAP-1 mAbs. VAP-1 inhibition by mAbs has been tested in several disease models (Tohka *et al.* 2001; Martelius *et al.* 2004; Bonder *et al.* 2005; Merinen *et al.* 2005). Blocking of VAP-1 with antibodies increases the rolling velocity, which further reduces firm adhesion and impairs the migration process of granulocytes (Tohka *et al.* 2001). A number of compounds to block the activity of SSAO/VAP-1 enzymes have been described. However, many of these compounds lack selectivity, have poor drug-like properties, such as low solubility or insufficient pharmacokinetics, and safety concerns, such as the presence of hydrazine groups.

Blocking with mAbs does not block the oxidase activity of VAP-1. A fully human monoclonal antibody, BTT-1023, specifically binds to the VAP-1 and blocks its function as an adhesion molecule. BTT-1023 is being investigated in small clinical trials in RA and psoriasis. Recently, the development of BTT-1023 has focused on the fibrotic diseases and it has been accepted for the Phase 2 clinical trials (Weston *et al.* 2015). Widely used inhibitors semicarbazide and hydroxylamine entirely inhibit the enzymatic activity of SSAO. BTT-2052 ((1*S*,2*S*)-2-(1-methylhydrazino)-1-indanol), also known as a SZE 5302, is a small-molecule indane hydrazine alcohol, which prevents leukocyte migration in experimental model of skin diseases. It has low inhibitory activity against MAO-A and MAO-B (Koskinen *et al.* 2004; Marttila-Ichihara *et al.* 2006).

Also many LJP series of inhibitors have been evaluated against VAP-1. LJP 1586 ((Z-3-fluoro-2-94-methoxybezyl)-allylamine hydrochloride) is a non-hydrazine compound and has remarkable specificity for VAP-1. LJP 1586 has no significant inhibition of cyclo-oxygenase-1 and -2 (COX-1 and COX-2). Its selectivity was 3500 fold greater than that of MAO-A. With a higher orally given dose, the inhibition of MAO-B could be seen. The results suggest that complete inhibition of SSAO can be achieved with at dose that does not affect other enzymes substantially (O'Rourke *et al.* 2008). LJP 1207 is a small-molecule compound containing a hydrazine functional group. It is an orally active, potent and selective inhibitor for SSAO, which blocks the SSAO mediated adhesion in the leukocyte adhesion cascade. Oral administration of LJP 1207 also reduces local inflammatory mediators, such as prostaglandin E_2 (PGE_2) and TNF-α. A

major disadvantage is that, in prolonged use, hydrazine derivative-compounds can cause toxicity (Salter-Cid *et al.* 2005; O'Rourke *et al.* 2007).

PXS-4681A   [(Z)-4-(2-(aminomethyl)-3-fluoroallyloxy)benzenesulfonamide hydrochloride] is an allylamine-based inhibitor against SSAO/VAP-1 with high selectivity for SSAO/VAP-1. In an experimental LPS-injured mouse model and carrageenan air pouch model, PXS-4681A reduced migration of neutrophils (Foot *et al.* 2013). PXS-4728A is a fluoro-allylamine and chemically similar to PXS-4681A. It is a highly selective inhibitor for SSAO/VAP-1 and able to diminish inflammation in various experimental lung inflammation models (Schilter *et al.* 2015).

2.4 Nuclear molecular imaging

Nuclear molecular imaging facilitates the visualization, characterization and measurements of biological processes in living subjects and offers a bridge between animal and human research (Schnöckel *et al.* 2010). It requires radiolabeled molecular probes that are called tracers. Intravenously administered tracers accumulate to target tissues in human or animal subjects. In nuclear imaging, cameras detectors detect gamma rays and the signal can be reconstructed to 2D- or 3D-images. The fusion of nuclear imaging with computed tomography (CT) or magnetic resonance imaging (MRI) provides more detailed functional and anatomical information (Wehrl *et al.* 2009). Emission computed tomography (ECT) is divided into two subtypes, positron PET and single photon emission tomography (SPECT), which are described more detailed in the following.

2.4.1 PET

The first PET study on human brain was performed in 1975 by Ter Pogossian (Ter-Pogossian *et al.* 1975). Today, PET is a routine diagnostic tool for many diseases. PET is a powerful non-invasive imaging method to detect several functional disorders like cancer, inflammation, infection, cardiac diseases and neurological diseases. It provides quantitative tomographic images and allows the determination of the time course *in vivo*. PET tracers are labeled with a positron emitting radio isotope. When the radionuclide decays, it emits positron that collides with the nearby electron and subsequently annihilates after travelling a short distance within the body. Each annihilation produces two 511 keV gamma rays that travel in opposite directions and can be detected by means of a PET camera with detectors surrounding the subject. PET isotopes can be

produced with a cyclotron or generator. Commonly used cyclotron produced short-lived positron emitting radioisotopes are [11]Carbon (^{11}C, $T_{1/2}$ 20 min), [13]Nitrogen (^{13}N, $T_{1/2}$ 10 min), [15]Oxygen (^{15}O, $T_{1/2}$ 2 min) and [18]Fluorine (^{18}F, $T_{1/2}$ 110 min). The positron's kinetic energy affects the distance the positron travels in the body and may degrade spatial resolution. [18]F is an ideal radionuclide because of its favorable positron energy (0.64 MeV) with a short range in tissues (0.27 mm) to provide high-resolution of PET images. It has also an acceptable radiation dosimetry and a relatively long half-life (110 min). Metallic radionuclides, such as [68]Gallium (^{68}Ga, 68 min), [64]Copper (^{64}Cu) and [86]Yttrium are produced with a generator, which facilitates radionuclide production in any radiochemical laboratory (Hutchins *et al.* 2008). Physical properties of generator produced ^{68}Ga and cyclotron produced ^{18}F are presented in Table 2.

[^{18}F]FDG is an analog of glucose in which the oxygen in C2 position is replaced with 18-fluorine. The uptake of [^{18}F]FDG is based on increased glucose uptake. Similar to glucose, [^{18}F]FDG is transported into the cell via glucose transport protein (GLUT). Inside the cell glucose and FDG are phosphorylated by hexokinase as a first step before glycolysis. FDG cannot enter into glycolysis and is trapped into the cell as a FDG-6-fosfate. [^{18}F]FDG PET is widely used diagnostic tool for detection, staging, restaging and therapy response assessment in cancer patient (Boellaard *et al.* 2015). Other common clinical indications of [^{18}F]FDG PET based on the 2013 EANM/SNMMI guidelines, in the field of inflammation/infection are sarcoidosis, peripheral bone osteomyelitis, suspected spinal infection, FUO and vasculitides (Jamar *et al.* 2013). [^{18}F]FDG PET imaging cannot differentiate inflammation and cancer, which is a risk for false-positive results. Another challenge with [^{18}F]FDG is the its high accumulation in heart and brain, if inflammation foci are near to these organs.

Table 2. Physical properties of ^{68}Ga and ^{18}F and mean positron ranges in soft tissue (Sanchez-Crespo 2013).

Radionuclide	Half-live (h)	Max energy (MeV)	Mean positron range (mm)
[68]Ga	1.1285	1.899	1.05
[18]F	1.8288	0.6355	0.27

2.4.2 SPECT

SPECT is a functional, non-invasive imaging method that detects gamma rays, high-energy photons that are emitted from the nucleus, and the gamma camera converts the photons from the source into a light pulse and subsequently into a voltage signal. The difference to planar imaging that images the subject only from one perspective is that the SPECT camera rotates around patient and record multiple images to be reconstructed into three-dimensional images. Most commonly used SPECT isotopes are ^{99m}Technetium (^{99m}Tc, $T_{1/2}$ 6 h), ^{123}Iodide (^{123}I, $T_{1/2}$ 13.2 h) and ^{111m}Indium (^{111m}In, $T_{1/2}$ 2.8 d). *In vitro* labeling of white blood cells (WBC), especially granulocytes, has been a gold standard for imaging of infectious patients. WBC labeling with ^{111}In (^{111}In-oxide) or ^{99m}Tc (^{99m}Tc-hexamethylpropyleneamine, ^{99m}Tc-HMPAO) and imaging with a gamma camera provide a useful method for diagnosing infections and inflammation. WBCs are first collected from the patient, then *in vitro* labeled either with ^{99m}Tc-hexamethylpropylene (HMPAO) or with ^{111}In-oxine and finally reinjected to the patient. The long half-live and high radiation exposure are disvantages of ^{111}In. ^{99m}Tc provides more optimal physical features and lower radiation exposure (Sovijärvi Anssi, et al. 2003). The normal bio-distribution of WBCs to the bone-marrow is a challenging factor.

SPECT imaging allows for dual-tracer imaging where two different radiotracers with different energies can be imaged simultaneously. With PET this is extremely difficult due to all PET tracers are in same energy (511 keV) level (Rahmim and Zaidi 2008). For example, in peri-prosthetic joint infections, the combined imaging of leukocyte-bone and leukocyte-bone marrow is used to discriminate if the uptake is derived from the bone/activated bone marrow or infection. Labeling of WBCs is also a time-consuming technique and handling the infected blood is a contamination risk in the laboratory.

PET is more quantitative imaging method than SPECT. SPECT has many variables that cause challenges, such as radionuclides with different photon energies, different collimators, potential different energy windows to be used and more moving parts in the imaging system. However, SPECT is transitioning from qualitative image reconstruction to the quantitative applications (Bailey and Willowson 2014). The lower cost of SPECT cameras facilitates the use of SPECT worldwide both in developing and developed countries. Longer half-lives of radionuclides create flexibility for scheduling and collaboration between hospitals and other research centers, including, for example, delivery of radiotracers from elsewhere, which means that is not necessary to have own

radiochemical facilities (Khalil *et al.* 2011; Bateman 2012). Common features of PET and SPECT are presented in Table 3.

Table 3. Common features of PET and SPECT (Massoud and Gambhir 2003; Khalil *et al.* 2011).

Imaging technique	Spatial resolution	Principal targets
PET	Clinical 4-6 mm Preclinical 1-2 mm	Metabolic, gene/reporter expression, receptor/ligand interaction, enzyme targeting
SPECT	Clinical 8-12 mm Preclinical $\leq$ 1 mm	Gene/reporter expression, receptor/ligand interaction

2.4.3 Nuclear imaging of adhesion molecules

Endothelium controls the homeostasis between blood and sub-endothelial structures. The activation of endothelium is an early event in the various pathogenesis of various diseases, for example, atherosclerosis and RA. Nuclear molecular imaging allows for the detection and monitoring of biological processes, for example, adhesion molecule expression on the endothelium. It can provide detailed knowledge at an early stage of the disease and thus promote more personalized therapy. Molecular nuclear imaging can provide specific monitoring of the progression of diseases across the species, which makes it a valuable tool for medical research.

2.4.3.1 Selectins

Selectins are upregulated on the activated endothelium (E- and P-selectin) and activated platelets (P-selectin) under inflammatory stimuli. E-selectin is upregulated on inflamed synovial membrane and in inflammatory bowel disease (IBD) (Bhatti *et al.* 1998; Garrood *et al.* 2009). Soluble E-selectin is also elevated in patients with a clinically active disease (Bhatti *et al.* 1998).

P- and E-selectins have elicited interest as a target for molecular imaging in atherosclerosis (Libby, DiCarli and Weissleder 2010). P-selectin is expressed on the activated endothelium and its counter receptor is PSGL-1. P-selectin is an

important molecular target in acute and chronic cardiovascular diseases, because it promotes interactions between platelets, leukocytes and endothelium. Fucoidan is a sulfated polysaccharide with nanomolar affinity to P-selectin. ^{99m}Tc-fucoidan has shown to be a promising imaging agent in experimental rat models of ischemia reperfusion and in platelet-rich arterial thrombi (Rouzet *et al.* 2011). Recently, flucoidan has also been successfully labeled with ^{68}Ga and shown to be a promising imaging agent in an experimental murine model of atherosclerosis (Li *et al.* 2014).

2.4.3.2 VCAM-1 and ICAM-1

VCAM-1 plays a major role in the development of the progression of atherosclerotic plaques and it is a well-recognized marker of atherosclerotic plaque vulnerability (Cybulsky *et al.* 2001). A synthetic VCAM-1 targeted PET imaging agent [18]F-4V and the PET signal correlated closely with mRNA level of VCAM-1 in aorta. [18]F-4V provided low background activity and correlated well with statin treatment, which is known to reduce VCAM-1 expression. VCAM-1 is associated with inflammation during myocardial infarction and cardiac transplant rejection (Nahrendorf *et al.* 2009). ICAM-1 is upregulated on endothelium in acute and chronic pulmonary diseases. In rats, ^{111}In labeled ICAM-1 antibody was able to detect an acute lung injury (Weiner *et al.* 1998). In mice, ^{64}Cu labeled ICAM-1 targeting nanoparticles have demonstrated proof-of-principle as good carriers to the lungs and are therefore promising for imaging respiratory diseases (Rossin *et al.* 2008).

2.4.3.3 Integrins

Integrins are cell adhesion receptors mediating cell-cell and cell-extracellular matrix contacts and they are involved in several steps in the leukocyte adhesion cascade as described earlier. Integrins are heterodimeric transmembrane receptors. These receptors consist of α- and ß-subunits, comprising at least 24 subtypes of integrins. Integrin triple peptide motif Arg-Gly-Asp (RGD) is recognized via eight integrins. Several imaging studies in cancer have reported good results, especially with $\alpha_v\beta_3$ integrin, which is upregulated in tumor angiogenesis and metastases. Integrins are also highly expressed during fibrosis, wound healing and inflammation (Beer and Schwaiger 2008). A large set of ^{68}Ga-labeled RGD peptides has been produced with bifunctional chelating agents and tested in experimental animal models (Eo and Jeong 2016). [^{18}F]Galacto-RGD was the first RGD PET tracer that was tested in humans, and it provided good target-to-background ratio in the cancer imaging (Beer *et al.* 2011).

Previously, Zhu and coworkers demonstrated preliminary proof-of-concept results of a PET tracer, [^{68}Ga]PRG2 that targets $\alpha_v\beta_3$ integrin and is specifically designed to detect angiogenesis, including patients with RA (Zhu *et al.* 2014).

2.4.3.4 VAP-1

Jaakkola and co-workers have demonstrated proof-of-principle for VAP-1 being a potential molecule for *in vivo* imaging of inflammation (Jaakkola *et al.* 2000). Later on, VAP-1 has shown to be a potential target for *in vivo* imaging in several preclinical settings (Jaakkola *et al.* 2000; Mäkinen *et al.* 2005; Lankinen *et al.* 2008; Ujula *et al.* 2009; Autio *et al.* 2010; Silvola *et al.* 2010; Aalto *et al.* 2011; Retamal *et al.* 2016). VAP-1 targeting tracer, ^{68}Ga-DOTAVAP-1 is a linear nine amino-acid peptide (GGGGKGGGG) containing DOTA-chelate and labeled with ^{68}Ga and has been promising imaging agent in turpentine-oil induced rat model and osteomyelitis model (Lankinen *et al.* 2008; Autio *et al.* 2010). BTT-1023 is a VAP-1 targeting fully human mAb, which can be labeled with ^{123}I and ^{124}I. [^{123}I]BTT-1023 detects positive vasculature in mild synovial inflammation (Autio *et al.* 2013). The sialic acid binding immunoglobulin like lectins (Siglecs) mediate cell-cell interactions through the recognition of sialylated glycoconjugates. Siglec-9 is found on distinct subsets of leukocytes, such as neutrophils, monocytes, NK-cells, B-cells and a minor subset of CD8+T cells (Zhang *et al.* 2000; Crocker, Paulson and Varki 2007). Siglec-9 is a natural leukocyte ligand of VAP-1. It is previously reported that Siglec-9 is upregulated rapidly on the leukocyte surface in response to inflammatory stimuli. The fragment of Siglec-9 used for PET imaging is a synthetic cyclic peptide CARLSLSWRGLTLCPSK, containing amino acids 283-297 from Siglec-9. Aalto and co-workers have shown that ^{68}Ga-labeled Siglec-9 can be used for the imaging of inflammation and cancer in experimental animal models (Aalto *et al.* 2011; Retamal *et al.* 2016). Siglec-9 can also be labeled with ^{18}F, which is a commonly applied form of any clinically approved PET tracers. ^{18}F has favorable physical properties and it facilitates high quality PET images. It has been shown that 5-deoxy-5-[^{18}F]fluoro-ribose, [^{18}F]FDR, is efficient for the conjugation of peptides (Li *et al.* 2014). The major advantage of ^{68}Ga as compared to ^{18}F is that it is available from in-house generators and can be produced in any radiochemical laboratory.

3. AIMS OF THE STUDY

The purpose of this study was to investigate the potential of radiolabeled Siglec-9 as VAP-1 targeting PET tracers to detect inflammation in various diseases.

The work was performed using different experimental disease models aimed specifically to:

1. Investigate the feasibility of [^{68}Ga]DOTA-Siglec-9 to detect inflammation caused by *Staphylococcus epidermidis*

2. Evaluate the ability of [^{68}Ga]DOTA-Siglec-9 to detect mild synovitis in PHA induced rabbit model in comparison to [^{18}F]FDG

3. Translate 5-deoxy-5-[^{18}F]fluororibose-Siglec-9 into the preclinical setting and evaluate its usefulness in comparison to [^{68}Ga]DOTA-Siglec-9

4. Investigate whether functionally active VAP-1 is expressed in atherosclerotic plaques and if [^{68}Ga]DOTA-Siglec-9 and [^{18}F]FDR-Siglec-9 PET can detect inflamed atherosclerotic plaques

4. MATERIALS AND METHODS

Ethical issues

Animal studies

All study protocols were approved by the Finnish National Animal Experiment Board (ELLA) and regional State Administrative Agency for Sothern Finland (ESAVI). All the animal experiments were done at the Central Animal Laboratory of the University of Turku. Analgesia, anesthesia and housing were incompliance with the institutional guidelines.

Human samples

Patient studies were conducted in accordance with the Declaration of Helsinki, and the study protocol was approved by the Ethics Committee of the Hospital District of Southwest Finland. All patients provided their written informed consent (Subprojects II and IV)

4.1 Radiochemistry

4.1.1 Synthesis of [^{68}Ga]DOTA-Siglec-9

^{68}Ga was obtained from a ^{68}Ge/^{68}Ga generator (Eckert & Ziegler, Valencia, CA, USA) by elution with 0.1 M HCl. ^{68}Ga eluate (0.5 mL, $280-360$ MBq) was mixed with 2-[4-(2-hydroxyethyl)piperazin-1-yl]ethanesulfonic acid (HEPES, 120 mg) to give a pH of approximately 4.1. DOTA-Siglec-9 peptide ($5-35$ nmol, $12-85$ µg, dissolved in deionized water to give a stock solution of 1 mM; Peptide Specialty Laboratories GmbH, Heidelberg, Germany) was added, and the reaction mixture was heated at 100 °C for 15 minutes. No further purification was performed. The radiochemical purity of ^{68}Ga-DOTA-Siglec-9 was determined by radiodetector-coupled reversed-phase high-performance liquid chromatography (radio-HPLC) (Jupiter C18 column, 4.6×150 mm, 300 Å, 5 µm; Phenomenex, Torrance, CA, USA). The HPLC conditions were as follows: flow rate = 1 mL/minute; $\lambda = 215$ nm; A = 0.1 % trifluoroacetic acid (TFA)/water; B = 0.1 % TFA/acetonitrile; gradient: during $0-2$ minutes 82 % A and 18 % B; during $2-11$ minutes from 82 % A and 18 % B to 40 % A and 60 % B; during $11-15$ minutes from 40 % A and 60 % B to 82 % A and 18 % B; during $15-20$ minutes 82 % A and 18 % B. The radio-HPLC system consisted of LaChrom Instruments (Hitachi; Merck, Darmstadt, Germany) and of a Radiomatic 150TR radioisotope detector (Packard, Meriden, CT, USA).

4.1.2 Synthesis of [18F]FDR-Siglec-9

The tracer [18F]FDR-Siglec-9 synthesis was based on a ligation reaction between aminooxy-functionalized peptide precursor and 5-deoxy-5-[18F]fluororibose ([18F]FDR), as previously reported. [18F]FDR is an aldose sugar and is able to form oxime ether bond with an alkoxyamine. To achieve efficient conjugation reaction at low substrate concentration, the synthesis was carried out at pH 4.6 and with aniline as a catalyst. This tracer was produced with a remote-controlled radiosynthesis device in a lead-shielded hot cell. Briefly, [18F]FDR as a prosthetic group was conjugated to the aminooxy-functionalized Siglec-9 peptide (0.3 mM, PolyPeptide Group, France) in anilinium buffer (0.3 M, pH 4.6) for 10 min at room temperature. The reaction mixture was subjected to high performance liquid chromatography (HPLC) purification with a Phenomenex Jupiter Proteo column (250 × 10 mm). [18F]FDR-Siglec-9 was formulated in phosphate-buffered saline (PBS) with a sterile filtration (0.22 μm) for injection.

4.2 Animal models

4.2.1 Animal model of osteomyelitis

Thirty adult male Sprague-Dawley rats (Harlan, Netherlands) used in this study. The rats' mean weight was (425 ± 37 g). The animals were divided in three groups (Table 3).

Table 4. Experimental design

	Group	CFU/ml	N
#1	*S. epidermidis*	3×10^8	10
#2	*S. aureus*	3×10^5	10
#3	No bacterium (control)	-	10

For surgery, the animals were anesthetized with a mixture of ketamine hydrochloride (Ketaminol® vet 50 mg/ml, Intervet International B.V., Boxmeer, Netherlands) and medetomidine hydrochloride (Cepetor vet 1 mg/ml, CP-Pharma Handelsgesellschaft mbH, Burgdorf, Germany). All the animals underwent surgical implantation of a sterile intravenous catheter into the medullary canal of the left tibia. In Groups 1 and 2 the implantation was followed by an injection,

via a sterile catheter of aqueous morrhuate and *S. epidermidis* or *S. aureus* suspension. In Group 3, an equal amount of sterile saline was injected via a sterile catheter. Two weeks after the surgery the animals were imaged with a small animal PET/CT scanner.

4.2.2 Animal model of rheumatoid arthritis

The sixteen male New Zealand rabbits (weight 3.2 ± 0.6) were intra-articulary injected with 80 µg phytohemagglutinin (Sigma-Aldrich, St Louis, MO, USA). The animals were anesthetized with ketamine (Ketalar® 15mg/kg, Pfizer, Dublin, Ireland) and medetomidine (Domitor®, 0.1mg/kg, Orion Pharma, Espoo, Finland). Inflammation was also detected with Gadolinium enhanced MRI. Imaging was performed with a Philips Ingenuity TF PET/MR (Philips Healthcare, Cleveland, OH, USA). Based on the results of a validation study 24 h time point was selected for further studies with [^{68}Ga]DOTA-Siglec-9.

4.2.3 Animal model of an acute sterile inflammation

Twenty-four hours before PET studies, sixteen healthy Sprague-Dawley rats (weight 349 ± 22.2) were subcutaneously (s.c.) injected with 0.05 ml of turpentine oil (Sigma-Aldrich, Seelze, Germany) in right foreleg in order to generate a sterile inflammation.

4.2.4 Animal model of atherosclerosis

6-month-old atherosclerotic (n=71 weight), low-density lipoprotein receptor deficient mice expressing only apolipoprotein B100 (LDLR$^{-/-}$ApoB$^{100/100}$, strain #003000; Jackson Laboratory, Bar Harbor, ME, USA) were fed with a Western-type diet (42 % calories from fat and 0.2 % from cholesterol, without sodium cholate; TD 88137, Harlan, Teklad, Harlan Laboratories, Madison, WI, USA). The diet started when the mice were 2 months old and lasted four months until the imaging experiments were performed. 2-month-old C57BL/6N mice (n=44) fed with a regular chow diet served as healthy, non-atherosclerotic controls.

4.3 PET studies

4.3.1 PET studies of osteomyelitis (Subproject I)

The imaging device was Inveon Multimodality PET/CT scanner (Siemens Medical Solutions, Knoxville, TN, USA). The spatial resolution of the PET system is approximately 1.4 mm. Two weeks after the surgery, rats were anesthetized with isoflurane and CT was performed for anatomical reference and

attenuation correction. Subsequently, the rats were intravenously injected with 19 ± 2.0 MBq of ^{68}Ga-DOTA-Siglec-9 via the tail vein and a 30-min PET acquisition in a list mode was performed. PET data were reconstructed iteratively with the ordered-subsets expectation maximization 3D algorithm. In the PET image analysis, regions of interest (ROIs) were defined in the proximal and distal part of the operated tibia, contralateral tibia and contralateral skeletal muscle using Inveon Research Workplace software (Siemens Medical Solutions, Malvern, PA, USA) (Figure 4.). The tracer accumulation was expressed as a standardized uptake value (SUV), calculated as [(average radioactivity within the ROI)/(injected radioactivity dose/rat body weight)]. The SUV_{ratios} between the operated tibia and the contralateral intact tibia and between the operated tibia and the contralateral muscle were calculated and used for intra- and inter-group comparisons.

Figure 4. A contour image of the operated tibia. ROIs were defined as proximal (ROI 1) and distal (ROI 2) parts.

After PET imaging, the animals were sacrificed. The tibias with intramedullary catheters were retrieved and sliced into five segments using sterile techniques (Figure 5). The first two segments were taken for histology, the third segment was taken for microbiological analyses, the fourth segment was used for PET *ex vivo* radioactivity measurements, and the fifth segment was prepared for fluorescence microscopy imaging of biofilm formation. Standard tissue samples (operated tibia and contralateral tibia, contralateral muscle, blood, heart, kidney, liver, lung, plasma and urine) were excised, weighed, and measured for total radioactivity using a gamma counter (1480 Wizard 3", PerkinElmer/Wallac, Turku, Finland). *Ex vivo* radioactivity measurements were corrected for the radionuclide decay to the time of injection. The radioactivity remaining in the tail was subtracted from the injected radioactivity. The tissue uptake of radioactivity was reported as a SUV and SUV_{ratios}.

Slice	Method
1	van Gieson staining
2	Hematoxylin and eosin staining
3	Microbiological verification
4	PET studies
5	Fluorescent microscopy
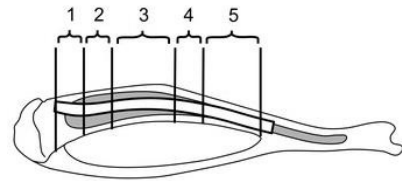
Figure 5. *Ex vivo* studies of operated tibia and a schematic illustration of the sliced segments

4.3.2 PET studies of rheumatoid arthritis (Subproject II)

The tracers were administered into each rabbit's ear vein. The 20 minute [^{18}F]FDG PET acquisition started at 40 minutes after the injection of the tracer. Based on validation study, 24h time point was selected for studies with [^{68}Ga]DOTA-Siglec-9. A dynamic 30-min [^{68}Ga]DOTA-Siglec-9 PET was performed for seven rabbits by using High Resolution Research Tomograph (HRRT; Siemens Medical Systems, Knoxville, TN, USA), a high resolution PET camera for human brain and small-animal PET-imaging with design features that enable high image spatial resolution (app. 2.5 mm). The data acquired in a list mode were iteratively reconstructed with a 3-D ordered subsets expectation-maximization algorithm with 8 iterations, 16 subsets, and a 2-mm full-width at half-maximum post-filter into 4×300 s time frames for [^{18}F]FDG and into 8×30 s, 6×60 s and 4×300 s time frames for [^{68}Ga]DOTA-Siglec-9. Ten minutes before sacrifice, the animals were i.v. injected with anti-VAP-1 antibody (BTT-1023, 1 mg/kg, Biotie Therapies Corp., Turku, Finland). The antibody binds to an epitope of luminal VAP-1, which is essential for PET imaging with Siglec-9. After PET imaging, all animals were sacrificed and various tissues were collected for *ex vivo* studies. Quantitative analyses were performed with Carimas 2.8 software (Turku PET Centre, Turku, Finland). ROIs were drawn in the inflamed knee, contralateral knee, femoral muscle and abdominal aorta (blood pool). The average radio activities were used for further analyses and the uptake was reported as a SUV.

Ex vivo distribution of [^{18}F]FDG and [^{68}Ga]DOTA-Siglec-9 was studied from several tissues with a gamma counter (1480 Wizard 3", PerkinElmer/Wallac, Turku,Finland). *Ex vivo* distribution of [^{68}Ga]DOTA-Siglec-9 was also studied with digital autoradiography of the inflamed and intact synovial tissue samples. For the autoradiography and further immunohistochemical analyses, tissue samples were frozen with dry ice, sectioned with cryomicrotome into 8 µm and 20 µm sections.

4.3.3 PET studies of an acute inflammation (Subprojects III and V)

In Subprojects III and V, sixteen adult rats were divided into two groups. In the first group, dynamic 60-min PET imaging was performed with [^{18}F]FDR-Siglec-9 (18.3 ± 5.1 MBq) for eight rats. In the other group, eight rats were i.v. administered with [^{68}Ga]DOTA-Siglec-9 (16 ± 2.9 MBq) and five of them were imaged with PET. PET imaging was performed with HRRT (Siemens Medical Systems, Knoxville, TN, USA). The PET data were reconstructed into 5×60 s and 11×300 s frames using an ordered-subsets expectation maximization 3D algorithm (OSEM3D). Using Carimas 2.9 software (Turku PET Centre, Turku, Finland), ROIs were drawn in the inflamed area, muscle, blood, liver, lungs, kidneys and urine. An estimation of human radiation dosimetry was calculated from the rat *in vivo* data by using OLINDA/EXM1.0 software (Vanderbilt University, Nashville, TN, USA) (Mikkola *et al.* 2014).

After PET imaging, the animals were sacrificed and several tissues were collected, weighted and measured with a gamma counter (1480 Wizard 3", PerkinElmer/Wallac, Turku,Finland). Results were expressed as a percentage of injected radioactivity per gram of tissue (%IA/g).

4.3.4 PET studies of atherosclerosis (Subprojects IV and V)

In Subprojects IV and V, the subsets of LDLR$^{-/-}$ApoB$^{100/100}$ mice (n=5) and healthy C57BL/6N (n=5) mice were imaged with a small animal PET/CT scanner (Inveon, Siemens Medical Solutions, Knoxville, TN, USA). Dynamic 60-min PET/CT imaging was performed with [^{68}Ga]DOTA-Siglec-9 peptide or [^{18}F]FDR-Siglec-9 and followed by contrast-enhanced CT angiography (eXIATM160XL, Binitio Biomedical Inc., Ottawa, ON, Canada). The PET data were iteratively reconstructed using an ordered-subsets expectation maximization 3D algorithm (OSEM3D with four iterations and six subsets) to yield 5×60 s, 1×300 s, 10×120 s, and 2×1800 s time frames (matrix size, $128 \times 128 \times 159$; pixel size, $0.776 \times 0.776 \times 0.796$ mm). CT images were reconstructed using a Feldkamp-based algorithm (matrix size, $768 \times 768 \times 923$; pixel size,

0.094 × 0.094 × 0.094 mm). PET/CT co-registration was done automatically and confirmed visually on the basis of anatomical landmarks. The quantitative PET image analysis was done by defining ROIs within aortic arch and the left ventricle of the heart. Time frames 10-20 min post-injection were used for PET image analysis and the results were expressed as SUVs and target-to-background ratios $SUV_{max, \text{ aortic arch}}/SUV_{mean, \text{ blood}}$.

In Subprojects IV and V, mice ($LDLR^{-/-}ApoB^{100/100}$, n = 22; C57BL/6N, n = 20) were injected with [^{68}Ga]DOTA-Siglec-9 (19 ± 5 MBq, n=22) or [^{18}F]FDR-Siglec-9 (18 ±5.1 MBq) under isoflurane anesthesia. At 25 min post injection the mice were sacrificed. First, a thoracic aorta was excised and rinsed with saline and after that, various other tissues were collected. Each collected tissue was separately weighted and the radioactivity measured with a gamma counter (Triathler 3″, Hidex, Turku, Finland). In Subproject IV, the hearts were preserved in formalin for further characterization of plaques in aortic root. After gamma counting, the aortas were frozen in isopentane and sequential longitudinal cryosections (20 and 8 µm) were cut using cryomicrotome at -15 ˚C. The *ex vivo* results were expressed as a percentage of the injected dose per gram (%IA/g).

The distributions of [^{68}Ga]DOTA-Siglec-9 and [^{18}F]FDR-Siglec-9 in the aorta were studied in more detail with digital autoradiography. ROIs were delineated in 1) plaques (excluding media) 2) the normal vessel wall, and 3) the adventitia.

In Subproject IV, the uptake of [^{68}Ga]DOTA-Siglec-9 and macrophage density in aortic plaques were compared. Macrophages were identified using 8 µm aorta cryosections that were immunohistochemically stained with a rat anti-mouse antibody (Clone M3/84, dilution 1:1000, BD Biosciences, Franklin Lakes, NJ, USA). Mac-3 positive areas in plaques were calculated using an automatic color deconvolution method and ImageJ v. 1.469 software (Fiji, National Institutes of Health, Bethesda, MD, USA). Uptakes of [^{68}Ga]DOTA-Siglec-9 were studied in the same areas using hematoxylin-eosin staining for reference.

In Subproject IV, a competition study was performed with $LDLR^{-/-}ApoB^{100/100}$ mice (n=5). Animals were injected with 500× excess of unlabeled synthetic Siglec-9 peptide (ChinaPeptides Co., Ltd., Shanghai, China), diluted in saline 10 minutes before the radiotracer administration. Subsequently, [^{68}Ga]DOTA-Siglec-9 (22 ± 9 MBq) was injected and studied as described above.

4.4 Immunohistochemistry of VAP-1

In Subprojects II, IV and V, the animals were intravenously (i.v.) injected with an anti-VAP-1 antibody ten minutes before sacrifice for detection of luminally expressed VAP-1. In Subprojects II, the rabbits' were i.v. injected with an anti-VAP-1 antibody (BTT-1023 1 mg/kg, Biotie Therapies Corp., Turku, Finland). In Subprojects IV and V, the mice were i.v. injected with monoclonal rat anti-mouse VAP-1 antibody (7–88, 1 mg/kg diluted in saline) antibody. After sacrifice, the rabbits inflamed synovium and mice aorta samples were frozen and cut into 8 μm longitudinal sections. Rabbit synovium sections were then incubated with the secondary antibody, fluorescein isothiocyanate (FITC)-conjugated anti-mouse IgG (Sigma-Aldrich, Seelze, Germany) with 5% rat serum for 30 min at room temperature, and finally, the sections were coated with Prolong Gold anti-fade reagent (Invitrogen Molecular Probes, Eugene, OR, USA). Mice sections were incubated for 30 min at room temperature in the dark with a secondary goat anti-rat antibody (working dilution, 5 μg/mL in phosphate-buffered saline (PBS) containing 5% normal mouse or human AB serum) conjugated to a fluorescent dye (Alexa Fluor 488; Invitrogen, Eugene, OR, USA).

In situ binding of Siglec-9 peptide was also studied in human rheumatoid synovium (Subproject II) and in frozen sections of human carotid endarterectomy samples (Subproject IV). Double-stainings were performed with biotinylated Siglec-9 (20 μg/ml; NeoMPS, Strasbourg, France) and anti-VAP-1 antibody (20 μg/ml; JG2.10 gift from E. Butcher, Stanford University, CA, USA). Streptavidin-Phycoerythrin (PE) was used with biotinylated Siglec-9. Fluorescence stainings of inflamed synovium were analyzed with Olympus 60X fluorescent microscope. For the human endarterectomy frozen sections, autofluorescence was distinguished from specific staining using the lambda scan mode and subsequent linear unmixing based on reference spectra. All fluorescent images were captured using a Zeiss LSM780 confocal microscope (Carl Zeiss MicroImaging GmbH, Jena, Germany).

4.5 Inhibition of VAP-1

Fifteen LDLR$^{-/-}$ApoB$^{100/100}$ mice were treated three times per week with intraperitoneal (i.p.) injections of a small molecule VAP-1 inhibitor, LJP 1586 ((Z-3-fluoro-2-(4-methoxybenzyl)allylamine hydrochloride; 0.5 mg/mL diluted in PBS; a kind gift from M. Linnik, La Jolla Pharmaceuticals, San Diego, CA, USA) at a dose of 5 mg/kg. A control subset of LDLR$^{-/-}$ApoB$^{100/100}$ mice (n=10)

were treated with saline (200µl). After treatment the animals were sacrificed and the hearts were collected, formalin-fixed and paraffin-embedded. Tissues were cut transversely into 5 µm sections at the level of coronary ostia. Each section was stained with Movat's pentachrome and intima-to-media ratios were determined with ImageJ v. 1.469 software (Fiji, National Institutes of Health, Bethesda, MD, USA) as described previously. Adjacent sections were stained with an anti-mouse Mac-3 antibody to detect activated macrophages.

4.6 Statistical analyses

All results are expressed as the mean ± SD with two significant figures. Normal distribution of the data was verified using Kolmogorov-Smirnov test. Non-paired data were compared between two groups using a t-test and between multiple groups using ANOVA with Tukey's correction. A paired t-test or Pearson's correlation analysis was used to compare paired data between two groups. A p-value < 0.05 was considered statistically significant.

5. RESULTS

5.1 Detection of biomaterial related peri-implant infections (Subproject I)

5.1.1 Histology and immunohistochemistry

The capability of *S. epidermidis* and *S. aureus* biofilm production and the sterility of the control group were verified with microbiological analyses. The extent of inflammation was also studied by hematoxylin-eosin and van Gieson stainings. Histologically, *S. epidermidis* infection was severe, whereas *S. aureus* signs of inflammation varied low to severe. In the sterile catheter group, low inflammatory reactions and new bone formations around the catheters were seen.

5.1.2 PET studies

PET/CT imaging with $[^{68}Ga]$DOTA-Siglec-9 detected inflammation/bone healing process in the bone implant rat model. Inflammatory response to a sterile catheter caused accumulation of $[^{68}Ga]$DOTA-Siglec-9 in the proximal (23.7 %, *p < 0.001*) and distal tibia (23.7 %, p < 0.001) compared to the contralateral intact tibia. In *S. epidermidis* group, the local uptake of $[^{68}Ga]$DOTA-Siglec-9 was significantly increased in both the proximal (SUV_{ratio} +58.1 %, *p = 0.009*) and distal (SUV_{ratio} +48.2 %, *p < 0.013*) tibia. In the operated tibia, the uptake was accumulated, especially in the proximal part. The difference between *S. epidermidis* and the control group (without bacterial infections) was statistically significant (*p = 0.005*). In *S. aureus* group, statistical significance between the operated and contralateral tibia was not achieved.

5.2 Detection of synovitis (Subproject II)

5.2.1 Histology and immunohistochemistry

Intra-articular injection of PHA caused a mild inflammation in the rabbit synovium. Hematoxylin-eosin stainings showed infiltration of inflammatory cells in the inflamed synovium. Luminal expression of VAP-1 was proved with intravenous injection of anti-VAP-1 antibody followed by an immunohistochemical staining with fluorescent secondary antibody. Double-stainings with biotinylated Siglec-9 and anti-VAP-1 showed co-localization in human inflamed synovium.

5.2.2 PET studies

Synovial inflammation was clearly visualized *in vivo* with $[^{18}F]$FDG, (Gd)-enhanced MRI and $[^{68}Ga]$DOTA-Siglec-9. *In vivo* inflamed-to-control joint SUV-ratio was 1.6 ± 0.2 (*p = 0.0020*) with $[^{18}F]$FDG PET and 1.2 ± 0.14 (*p <*

0.001) with [68Ga]DOTA-Siglec-9 PET (Figure 6. A-C). The *ex vivo* results showed comparable uptakes between the inflamed synovium and intact contralateral synovium with [18F]FDG PET (1.5 ± 0.2, P = 0.014) and [68Ga]DOTA-Siglec-9 PET (1.7 ± 0.4, P = 0.0035). However, the difference was not statistically significant (*p = 0.32*). The results of *in vivo* and *ex vivo* PET correlated well, [18F]FDG; r = 0.84, *p < 0.001*, [68Ga]DOTA-Siglec-9; r = 0.72, *p > 0.001*. Digital autoradiography results were in line with *in vivo* and *ex vivo* [68Ga]DOTA-Siglec-9 PET results and showed a statistically significant uptake in the inflamed synovium (2.3 ± 1.2) as compared to the control synovium (1.2 ± 0.52, *p = 0.020*). (Figure 6. D)
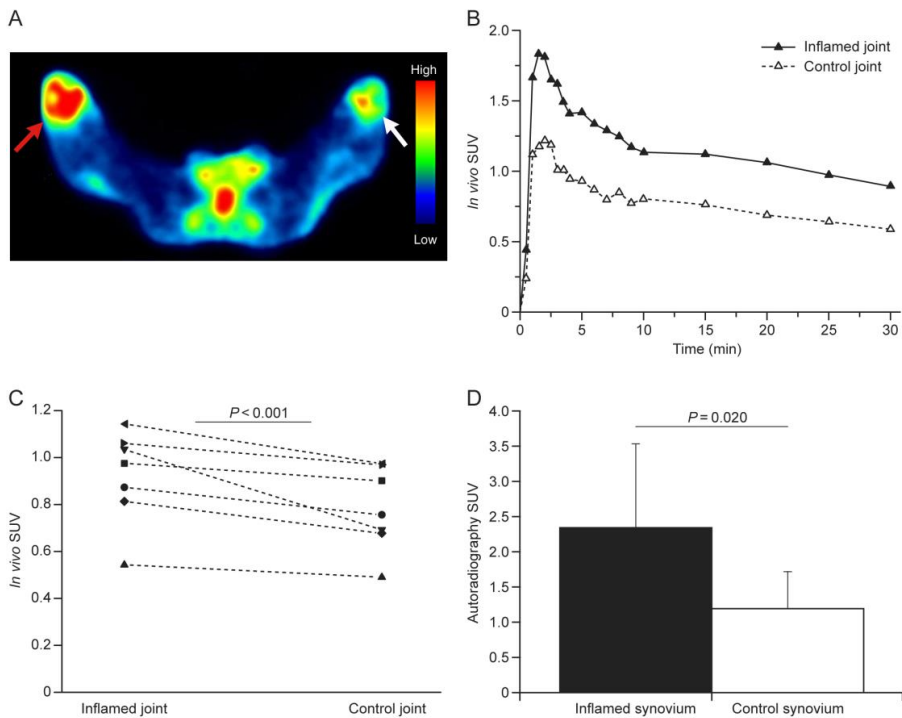
Figure 6. PET results of PHA induced synovitis in a rabbit model A) A representative [68Ga]DOTA-Siglec-9 PET image of the PHA induced rabbit model and B) its time-activity curve. C) *In vivo* PET showed significantly higher uptake in the inflamed synovium compared to the control joint. D) Digital autoradiography showed significantly higher uptake in the inflamed synovium.

5.3 Detection of an acute sterile inflammation (Subproject III and V)

5.3.1 PET studies

Hematoxylin-eosin staining showed the common hallmarks of acute inflammation, such as edema, and the infiltration of neutrophils in inflamed tissue. Turpentine oil-induced inflammation was clearly visualized with [^{18}F]FDR-Siglec-9 (SUV$_{mean,10\text{-}60min}$ 0.77 ± 0.22) and [^{68}Ga]DOTA-Siglec-9 (SUV$_{mean,inflammation}$ 0.77 ± 0.31) (Figure 7). Time-activity-curves of the inflamed tissue were comparable (*p = 0.29*) between [^{18}F]FDR-Siglec-9 and [^{68}Ga]DOTA-Siglec-9. Both tracers peaked about 10 min after the i.v. bolus injection, with a slow decrease thereafter. In the inflamed tissue, the *ex vivo* results showed significantly higher (*p = 0.013*) uptake with [^{18}F]FDR-Siglec-9 (0.19 ± 0.053 %IA/g) than with [^{68}Ga]DOTA-Siglec-9 (0.12 ± 0.032 %IA/g). The [^{18}F]FDR-Siglec-9 PET results were partly published in Subproject III and more detailed in Subproject V.
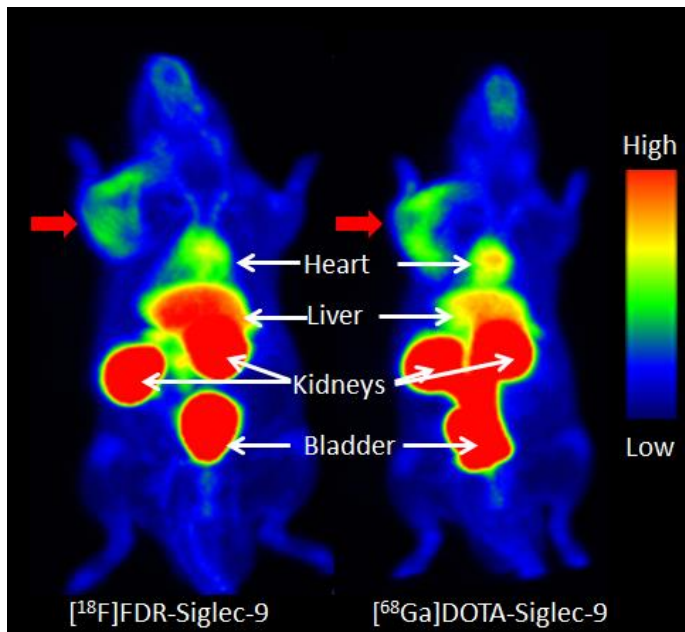
Figure 7. Representative images of [^{18}F]FDR-Siglec-9 and [^{68}Ga]DOTA-Siglec-9 PET images of an acute inflammation in a rat model. Red arrows show inflamed areas in the rats' forelegs.

5.3.2 Human radiation dosimetry

An effective dose of 70 kg human adult was extrapolated from the *in vivo* results of the rat model. The effective dose was 0.022 ± 0.0042 mSv/MBq for [^{18}F]FDR-Siglec-9 and 0.024 ± 0.0041 mSv/MBq for [^{68}Ga]DOTA-Siglec-9. The most critical organs were kidneys for [^{18}F]FDR-Siglec-9 and urinary bladder wall for [^{68}Ga]DOTA-Siglec-9.

5.4 Detection of inflamed atherosclerotic plaques (Subprojects IV and V)

5.4.1 Histology and immunohistochemistry

Luminal expression of VAP-1 in inflamed atherosclerotic plaques was verified in LDLR$^{-/-}$ApoB$^{100/100}$ mice. Intravenously injected anti-VAP-1 antibody was administered 10 minutes before the sacrifice and frozen sections of mice aortas were stained with the fluorescent-labeled secondary antibody. Based on the detection of fluorescence, VAP-1 was expressed on the luminal endothelial cells lining the aortic plaques. Double-staining of human carotid artery samples showed co-localization of Siglec-9 with VAP-1.

5.4.2 PET studies with [^{68}Ga]DOTA-Siglec-9

Atherosclerotic lesions were detectable in PET with [^{68}Ga]DOTA-Siglec-9 at 10-20 min post-injection. The ratio between plaque ($SUV_{max, \text{ aortic arch}}$) and blood ($SUV_{mean}$) was 1.7 ± 0.22, *p = 0.00029*.

The *ex vivo* result showed that the uptake in aorta was significantly higher in the atherosclerotic LDLR$^{-/-}$ApoB$^{100/100}$ ($0.83 \pm 0.33\%$IA/g) aortas than in controls (0.46 ± 0.10 %IA/g), *p = 0.0010*. *The ex vivo* biodistribution results of [^{68}Ga]DOTA-Siglec-9 in the LDLR$^{-/-}$ApoB$^{100/100}$ and control mice are presented in Table 5. In the competition study, the excess of unlabeled Siglec-9 reduced the uptake in LDLR$^{-/-}$ApoB$^{100/100}$ aortas by 42 %, to the same level as in controls (0.48 ± 0.066 %IA/g).

The autoradiography results showed significantly higher uptake in atherosclerotic mice than in controls. The competition assay reduced the uptake in plaques by 48%, but the uptake in normal vessel wall remained unchanged. The uptake of [^{68}Ga]DOTA-Siglec-9 correlated with Mac-3 positive macrophages (r=0.58, *p = 0.022*).

5.4.3 PET studies with [^{18}F]FDR-Siglec-9

Atherosclerotic plaques were detectable in *in vivo* PET with [^{18}F]FDR-Siglec-9. The ratio between $SUV_{max, aortic\ arch}$ and $blood_{mean}$ was 1.6 ± 0.078. The *ex vivo* gamma counting showed that the uptake was significantly higher in the atherosclerotic LDLR$^{-/-}$ApoB$^{100/100}$ (0.93 ± 0.38 %ID/g) than in controls (0.52 ± 0.23 %ID/g ($p = 0.0015$). *The ex vivo* biodistribution results of [^{68}F]FDR-Siglec-9 in the LDLR$^{-/-}$ApoB$^{100/100}$ and control mice are presented in Table 5

Digital autoradiography showed significantly higher uptakes in plaques than in normal vessel wall or adventitia in atherosclerotic plaques in LDLR$^{-/-}$ApoB$^{100/100}$ mice. In LDLR$^{-/-}$ApoB$^{100/100}$ mice, the plaque-to-wall ratio was 1.9 ± 0.23 ($p < 0.001$) and plaque-to-adventitia ratio 2.2 ± 0.53 ($p < 0.001$). In control mice, the uptake of [^{18}F]FDR-Siglec-9 in healthy vessel wall was similar to that in the atherosclerotic mice

5.4.4 Inhibition of VAP-1

Functional activity of VAP-1 in atherosclerotic plaques was studied with a small-molecule inhibitor LJP 1586. Mac-3 positive macrophages reduced by 46 % as compared to the saline group (inhibitor, $8.2\% \pm 3.5\%$ *vs.* saline, $15\% \pm 5.1\%$; $p < 0.0001$). The treatment with the inhibitor had no effect on the plaque size, determined as the intima-media ratio (inhibitor, 1.9 ± 0.8 vs. saline, 1.5 ± 0.6; $p = 0.15$), body weight or plasma lipid levels.

Table 5. [^{68}Ga]DOTA-Siglec-9 and [^{18}F]FDR-Siglec-9 *ex vivo* biodistribution in atherosclerotic LDLR$^{-/-}$ApoB$^{100/100}$ and healthy C57Bl/N6 mice. The results are expressed as %IA/g.

Organ	[^{68}Ga]DOTA-Siglec-9 LDLR$^{-/-}$ApoB$^{100/100}$	[^{68}Ga]DOTA-Siglec-9 C57BL/6N	*P-value*	[^{18}F]FDR-Siglec-9 LDLR$^{-/-}$ApoB$^{100/100}$	[^{18}F]FDR-Siglec-9 C57BL/6N	*P-value*
Aorta	0.83 ± 0.33	0.46 ± 0.10	**	0.93 ± 0.38	0.52 ± 0.23	**
BAT	0.77 ± 1.1	0.54 ± 0.25	*NS*	0.57 ± 1.4	0.45 ± 0.13	*NS*
Blood	3.0 ± 1.3	1.5 ± 0.63	***	3.2 ± 0.82	2.1 ± 0.59	***
Brain	0.10 ± 0.050	0.06 ± 0.020	***	0.15 ± 0.060	0.11 ± 0.048	*
Heart	0.59 ± 0.27	0.29 ± 0.12	***	0.62 ± 0.28	0.34 ± 0.082	**
Kidney	33 ± 18	33 ± 15	*NS*	44 ± 26	43 ± 25	*NS*
Liver	4.0 ± 3.1	4.0 ± 2.3	*NS*	3.0 ± 0.97	3.5 ± 2.3	*NS*
Lungs	1.5 ± 0.61	1.4 ± 0.99	*NS*	2.4 ± 1.1	1.5 ± 0.45	*
Muscle	0.50 ± 0.23	0.28 ± 0.13	**	0.62 ± 0.20	0.43 ± 0.13	**
Pancreas	0.76 ± 0.33	0.33 ± 0.15	***	0.82 ± 0.28	0.57 ± 0.18	*
Plasma	6.1 ± 7.0	1.5 ± 0.33	-	5.7 ± 1.4	3.8 ± 0.62	***
Small intestine	0.81 ± 0.49	0.90 ± 0.90	***	1.6 ± 0.49	0.79 ± 0.29	***
Spleen	2.8 ± 1.9	2.2 ± 1.2	*NS*	1.1 ± 0.28	0.62 ± 0.32	*NS*
Thymus	0.68 ± 0.53	0.36 ± 0.16	*	0.69 ± 0.19	0.43 ± 0.089	***
Urine	130 ± 99	83 ± 76	**	470 ± 370	610 ± 340	*NS*
WAT	0.37 ± 0.21	0.34 ± 0.27	*NS*	0.72 ± 0.66	0.63 ± 0.37	*NS*

Values are expressed as a mean ± SD, *P < 0.05, **P < 0.01, ***P < 0.001
BAT = Brown adipose tissue, WAT= white adipose tissue

6. DISCUSSION

6.1 Detection of peri-implant tissue responses

In Subproject I, the aim was to evaluate the capability of the novel tool, [^{68}Ga]DOTA-Siglec-9 PET, to detect inflammatory response to *S .epidermidis* infections. The results indicated that VAP-1 could be a suitable target to detect inflammatory response in peri-implant tissue infections caused by *S. epidermidis*.

In nosocomial infections, clinically indolent *S. epidermidis* is introduced as the most common cause of biomaterial related infection (Otto 2009). In Subproject I, *S. aureus* and *S. epidermidis* were used to cause a peri-implant tissue response in rat tibia. Clinically isolated T-54580 *S. epidermidis* and 52/52A/80 *S. aureus* strains were used in Subproject I. The capacity to produce biofilm was tested for each bacterial strain before the *in vivo* studies. The bacterial concentrations of *S. epidermidis* and *S. aureus* were selected on the basis of previously reported studies (An and Friedman 1998; Sakaeda 1988; Lambe *et al.* 1991; Del Pozo *et al.* 2009; Alt *et al.* 2011). The selected dose may be the reason why only 60-70 % of the animals were found to be positive for *S. aureus* bacterial growth. Previously, in an experimental osteomyelitis study, Mäkinen and co-workers applied a higher *S. aureus* concentration in rats tibia, which resulted in severe osteomyelitis in all cases (Mäkinen *et al.* 2005). This suggests that the *S. aureus* concentration used in Subproject I was too low.

Silicon catheter is a commonly used foreign body in experimental osteomyelitis studies (Mayberry-Carson *et al.* 1984; Lambe *et al.* 1991; An, Kang and Arciola 2006). To our knowledge, Subproject I was the first study to report on the use of silicon catheters in rat models of osteomyelitis. The major advantage of the use of catheter is the closed direct injection of the inoculum into the close space of the medullary canal. Medical catheters are a common reason for hospital infections, providing favorable surface for bacterial colonization and biofilm production (Dohnt *et al.* 2011; Brooks and Jefferson 2012). *S. epidermidis* is named as a leading pathogen of biomaterial-related nosocomial infections, including peri-prosthetic joint infections (Zimmerli, Trampuz and Ochsner 2004; Kwakman *et al.* 2006).

In Subproject I, before the inoculation of the bacteria, sodium morrhuate was injected via the catheter. Sodium morrhuate is a sclerosing agent, which causes aseptic bone necrosis and increases the probability of local bone infection. The use of sodium morrhuate is contested. It is known that sodium morrhuate induces

ischemia and bone marrow necrosis and subsequent bone repair process can misinterpret diagnostic imaging, especially at the early stage after inoculation (Volk *et al.* 1994). In our work, animals were pretreated with sodium morrhuate to confirm the reproducible induction of osteomyelitis and usually it defenses host response in order to reduce the number of bacteria to produce infection. The effects of sodium morrhuate are frequently applied in studies that are focused on diagnostic imaging (Hienz *et al.* 1995; Mäkinen *et al.* 2005; Lankinen *et al.* 2008, 2012; Ujula *et al.* 2009). Lankinen and co-workers showed that other VAP-1 targeting tracer, ^{68}Ga-DOTAVAP-P1, does not specifically accumulate into infectious site and it rather describes the rate of inflammation in experimental rabbit model (Lankinen *et al.* 2008). In study I, the possibility that inflammation is partly caused by sodium morrhuate cannot be fully ruled out. Because sodium morrhuate causes aseptic bone necrosis and healing is closely linked to inflammation/leukocyte infiltration, it may impair the differentiation between infection and healing in imaging studies. The results suggest, however, that the effect of the sclerosing agent is marginal because no statistically significant difference was seen between the *S. aureus* group with sodium morrhuate and the sterile implant group without sodium morrhuate. This conclusion is uncertain because of the small amount of animals in *S. aureus* group (n = 7 and only 70 % were *S. aureus* positive) that misinterprets statistical analysis. This study was conducted only in one time-point, 2 weeks after operation. Imaging in various time-points could be helpful to recognize infection and healing in this type of experimental imaging study.

Diagnostic discrimination between prosthetic infection and loosening is a major problem in joint replacements. [^{18}F]FDG has a limited value for differentiation of an infectious bacterial inflammatory process and a healing process involving inflammatory phases (De Winter *et al.* 2002; Koort *et al.* 2004). In a previous study with an experimental rabbit model, it was found that [^{18}F]FDG PET is highly effective in the detection of *S. aureus* osteomyelitis, the evaluation of the prevention of *S. aureus* biomaterial-related infections and the evaluation of treatment response to local therapy of *S. aureus* osteomyelitis (Koort *et al.* 2004; Lankinen *et al.* 2012). In contrast, a low [^{18}F]FDG uptake in a sub-acute peri-implant *S. epidermidis* infection in a rabbit osteomyelitis model has been reported (Lankinen *et al.* 2012). Mäkinen and co-workers have reported promising results of ^{68}Ga imaging of bone infections (Mäkinen *et al.* 2005).

In a rat osteomyelitis model, Lankinen and co-workers showed that a VAP-1 targeted peptide called [^{68}Ga]DOTAVAP-P1 is capable of differentiating

bacterial inflammation and the inflammatory phase of healing bone and describing the rate of the inflammatory/infectious reaction (Lankinen *et al.* 2008). Ujula and co-workers published proof-of-concept that infection-induced VAP-1 can be specifically targeted with [^{68}Ga]DOTAVAP-P1 and they encouraged further development of [^{68}Ga]DOTA-peptides (Ujula *et al.* 2009). In Subproject I, [^{68}Ga]DOTA-Siglec-9 was able to detect inflammation caused by *S. epidermidis*. In this study the *S. epidermidis* infections were severe and did not reflect clinically typical low-grade *S. epidermidis* infection. We concluded that [^{68}Ga]DOTA-Siglec-9 is able to detects *S. epidermidis* infection in rat osteomyelitis model. Because the study did not stimulate the clinically typical *S. epidermidis* infection it is still uncertain if the [^{68}Ga]DOTA-Siglec-9 can detect low-grade *S. epidermidis* infection. The endothelial molecules guiding the migration of leukocytes to sites of inflammation and infection are practically taken the same as infection always has inflammatory components. Since [^{68}Ga]DOTA-Siglec-9 uptake is based on the inflammation, it will be a challenge to differentiate inflammation caused by bacterial infection and aseptic inflammatory processes caused by the loosening of the joint prostheses (Stumpe *et al.* 2004; Love and Palestro 2016). However, Subproject I shows that [^{68}Ga]DOTA-Siglec-9 PET/CT may be a promising tool for the detection of inflammation caused by biomaterial-related bacterial infections. Optimization of the study protocol would be the first step to further evaluate the usefulness of [^{68}Ga]DOTA-Siglec-9 as a clinical tool.

6.2 Detection of synovitis

Early diagnosis of RA is essential in order to optimize and individualize therapy before structural damages occur (Mountz, Alavi and Mountz 2012). The purpose of Subproject II was to evaluate the feasibility of [^{68}Ga]DOTA-Siglec-9 PET in acute synovitis in a rabbit model and to compare these results with [^{18}F]FDG.

In Subproject II, the synovitis was induced with phytohemagglutinin (PHA). The first set of animals were evaluated with [^{18}F]FDG PET at 8 h and 24 h after PHA induction. The amount of PHA was based on earlier studies of VAP-1 in rabbit, dogs and pigs (Jaakkola *et al.* 2000; Autio *et al.* 2013). PHA is a toxic lectin, which is derived from plants. It is a mitogenic substance, contributing to the stimulation of T-cells to undergo mitosis (Sharon and Lis 2004). In Subproject II, the common features of inflammation, such as heat, redness and swelling, were observed in joints already at 8 h after PHA induction but at this timepoint, the [^{18}F]FDG PET did not show any significant difference in comparison to the contralateral knee. However, [^{18}F]FDG uptake was significantly higher 24 h after

PHA induction, as compared to the contralateral knee and therefore 24 h timepoint was chosen for further studies with [^{68}Ga]DOTA-Siglec-9. Also the histochemical staining supported our findings with [^{18}F]FDG. In addition, Gadolinium-enhanced MRI indicated a clear inflammation in PHA treated knee at 24 h.

Many different experimental models with animals, including mice, rats, rabbits and monkeys, have been used to simulate human RA (Trentham, Townes and Kang 1977; Yoo *et al.* 1988; Lin *et al.* 2007). In Subproject II, rabbit was chosen because the size of the rabbit joint is better suited for *in vivo* imaging, as compared to rodent joints. It is also reported that rabbit VAP-1 is sufficiently homologous with human VAP-1 and can be detected with some of the existing antibodies against human VAP-1 (Salmi and Jalkanen 2001; Autio *et al.* 2013). In a previous study, we used the same animal model and demonstrated the imaging of synovial inflammation with fully human anti-VAP-1 antibody [^{123}I]BTT-1023 (Autio *et al.* 2013). The *ex vivo* measured inflamed-to-contralateral synovium SUV ratios of [^{68}Ga]DOTA-Siglec-9 (1.7 ± 0.44) were in line with those for ^{123}I-BTT-1023 (1.7 ± 0.5). The luminal expression of VAP-1 is crucial for *in vivo* imaging with VAP-1 targeted tracers. In Subproject II, the luminal expression of VAP-1 was studied with fluorescence-based immunohistochemical stainings. Anti-VAP-1 antibody was given 10 min before the animals' sacrifice and the tissue sections were stained with a secondary antibody. Immunohistochemical stainings verified the luminal expression of VAP-1 on the endothelial cell surface. A few VAP-1 positive vessels were also found in the healthy synovium, which was probably due to a systemic response to chemically induced inflammation in the rabbit model. VAP-1 positive vessels have not been found in healthy synovial tissue in humans.

For many years bone, scintigraphy was the only available nuclear imaging technique for RA. Currently, several radiopharmaceuticals have been developed and tested for quantitative imaging of RA. PET/CT, SPECT/CT and PET/MRI may provide important molecular information for the detection of early inflammatory activity, the prediction and monitoring of response to treatment and optimal treatments for each patient (Rosado-de-Castro *et al.* 2014). It is reported that [^{18}F]FDG PET combined with well-established MRI is a sensitive modality for imaging RA (Miese *et al.* 2011). [^{11}C]Choline (Roivainen *et al.* 2003) and [^{11}C](R)-PK11195 PET/CT (van der Laken *et al.* 2008) have shown the most promising results in patients with RA. However, the short half-live of ^{11}C (20.4 min) and the rapid *in vivo* metabolism limit the use of these tracers. In addition,

promising results are published for the imaging of synovial angiogenesis with RGD peptides (Wilder 2002; Zhu *et al.* 2014). Several macrophage-targeting tracers are also under preclinical evaluation (Gent *et al.* 2013, 2014). Leukocyte-homing associated adhesion molecules, for example E-selectin and ICAM-1, have been investigated for *in vivo* imaging of inflammation in RA (Gompels *et al.* 2011; Blezer *et al.* 2015). According to our studies, VAP-1 is a promising target both for anti-inflammatory therapy and *in vivo* imaging. The new tracer, [^{68}Ga]DOTA Siglec-9 binds to the enzymatic groove of VAP-1, leaving the antibody binding site unoccupied and therapeutically accessible. Our results revealed that the uptake of [^{68}Ga]DOTA-Siglec-9 was comparable to [^{18}F]FDG in PHA-induced synovitis in rabbits. Further investigations are needed to clarify which tracer would perform best for the evaluation of anti-inflammatory therapy in man.

6.3 Detection of an acute sterile inflammation

In Subproject V, the experimental animal model with the turpentine oil-induced inflammation showed common signs of inflammation, such as heat, pain, redness and swelling in the inflamed area. Histologically, the infiltration of neutrophils was clearly visualized. This animal model is easy to implement, allowing good reproduction and usefulness for the evaluation of various tracers' capability to detect inflammation (Yamada *et al.* 1995; Autio *et al.* 2010, 2011, 2014; Aalto *et al.* 2011). However, increased blood flow and extensive oedema in inflamed tissues may cause challenges in terms of separating the PET signal between target and blood background.

Previously, Autio and co-workers have shown that luminal VAP-1 is expressed in the turpentine oil-induced rat model (Autio et al. 2010). In the current studies, both [^{68}Ga]DOTA-Siglec-9 and [^{18}F]FDR-Siglec-9 showed similar accumulation patterns in inflamed areas (Subprojects III and V). The uptake in the inflamed tissue was also higher and statistically significant as compared to blood with both tracers. Compared to the previous VAP-1 targeting PET studies with turpentine oil-induced rat model, the *in vivo* SUVs from inflamed area were 0.33 ± 0.07, 0.53 ± 0.01, 0.46 ± 0.06 and 0.43 ± 0.1 for [^{68}Ga]DOTAVAP-P1, [^{68}Ga]DOTAVAP-PEG-P1, [^{68}Ga]DOTA-Siglec-9 and [^{18}F]FDR-Siglec-9, respectively, at 60 min after injection (Autio *et al.* 2010, 2011). The reason why the uptake of [^{18}F]FDR-Siglec-9 was higher in several organs compared to the [^{68}Ga]DOTA-Siglec-9 is unclear. The uptake of may be increased because the beneficial impact of glycosylated peptides of glycosylation on *in vivo* pharmacokinetics of peptide tracers (Li *et al.* 2014). The *in vivo* stability also

remains unclear. However, in vivo imaging and *ex vivo* biodistribution showed low uptake in bone, which suggest that the tracers is not totally degraded.

Human radiation dosimetry was extrapolated from the rat data. The primary sites of radioactivity uptake in rats were liver, kidneys and urinary bladder and these organs were clearly visualized in PET images. The most critical organs were kidneys for [18F]FDR-Siglec-9 and urinary bladder wall for [68Ga]DOTA-Siglec-9. Effective doses were low as compared to, for example, [18F]FDG (ICRP publication 1998) and [68Ga]DOTANOC (Pettinato *et al.* 2008). The human radiation dosimetry is only an estimation from the rat data. The *in vivo* stability of [68Ga]DOTA-Siglec-9 and [18F]FDR-Siglec-9 is still uncertain and its determination would be critical information for reliable extrapolation of human radiation dosimetry. Our tracer is an amino acid sequence from human natural leukocyte ligand, Siglec-9. The corresponding leukocyte ligand for human Siglec-9 in rodents is Siglec-E (Aalto *et al.* 2011). This is also an uncertain factor concerning tracers' *in vivo* stability in animal studies.

6.4 Detection of atherosclerotic plaques

Our aim was to clarify if the functionally active VAP-1 is expressed in atherosclerotic lesions (Subproject IV) and if so, whether it could be targeted with PET (Subprojects IV and V). The Subproject IV provided evidence that VAP-1 is indeed a potential molecule for both imaging and anti-inflammatory therapy of atherosclerotic lesions. The luminal expression of VAP-1 was verified with fluorescence-based immunohistochemistry (Subproject IV) in LDLR^{-/-} ApoB[100/100] mice. Our results also showed that healthy, non-atherosclerotic vessel wall was VAP-1 negative. In addition, our immunohistochemical stainings confirmed that VAP-1 is expressed in human intra-plaque neovessels as previously reported by Teng and co-workers (Teng *et al.* 2012). Notably, our results revealed that the focal uptake of VAP-1 in atherosclerotic plaques correlated with the density of macrophages in mice, and the inhibition of VAP-1 with LJP 1586 reduced the density of macrophages in atherosclerotic lesions.

Endothelial activation plays a crucial role in the development of atherosclerosis. Several studies have demonstrated that endothelial cells express endothelial adhesion molecules on atherosclerotic arteries in both humans and animals (Ling, Nheu and Komesaroff 2012; Drechsler and Soehnlein 2013; Figueroa-Vega, Moreno-Frías and Malacara 2015). The expression of VAP-1 is reported in atherosclerotic lesions in humans and rabbits (Anger *et al.* 2007; Bulgarelli *et al.* 2012). Leukocytes, especially macrophages are key players in atherosclerosis

(Swirski and Nahrendorf 2013). In Subproject IV, we showed that the uptake of [^{68}Ga]DOTA-Siglec-9 is associated with the density of Mac-3-positive macrophages. The *in vivo* specificity of [^{68}Ga]DOTA-Siglec-9 was also tested with a competitive binding assay in atherosclerotic mice, and the co-localization of anti-VAP-1 antibody and Siglec-9 was verified in human atherosclerotic plaques *in situ*. The results proved that the plaque uptake of [^{68}Ga]DOTA-Siglec-9 peptide is specific for VAP-1 in LDL$^{-/-}$ApoB$^{100/100}$ mice. The results were in line with previously reported specificity results (Aalto *et al.* 2011). The co-localization of anti-VAP-1 antibody and Siglec-9 in human atherosclerotic plaques was clearly visualized with fluorescence-based immunohistochemistry thus further strengthening the concept of VAP-1-targeted [^{68}Ga]DOTA-Siglec-9 imaging of inflamed plaques.

Many non-invasive imaging modalities have been used to detect adhesion molecules in atherosclerotic inflammation (Kelly *et al.* 2005; Nahrendorf *et al.* 2006; Dimastromatteo *et al.* 2013; Sadat *et al.* 2014). In Subprojects IV and V, *in vivo* PET with [^{68}Ga]DOTA-Siglec-9 and [^{18}F]FDR-Siglec-9 showed moderate uptake in LDLR$^{-/-}$ApoB$^{100/100}$ mice aorta. The small size of the analyzed ROIs, limited resolution of the imaging device and partial volume effect cause difficulties to get reliable *in vivo* results even with ^{18}F. Also, intra-plaque neovessels are rarely found in mice, which makes *in vivo* imaging of atherosclerosis in mice even more challenging (Heinonen *et al.* 2007).

However, only few papers report on the imaging of atherosclerosis using and adhesion molecule-targeting PET probe. Nahrendorf and co-workers reported *in vivo* detection of VCAM-1 with [^{18}F]4V PET probe in the mouse aortic root (Nahrendorf *et al.* 2009). With [^{18}F]4V PET, the aortic root-to-blood ratio was approximately 2 at 4 h post-injection, which is comparable to our results, namely 1.7 with [^{68}Ga]DOTA-Siglec-9 and 1.6 with [^{18}F]FDR-Siglec-9. Nakamura and co-workers evaluated [^{64}Cu]DOTA-anti-P-selectin PET tracer in atherosclerotic mice (Nakamura *et al.* 2013). The long physical half-live (12.7 h) and high radiation exposure of ^{64}Cu limits its use in humans. In a recent report, ^{18}F-labeled anti-VCAM-1 nanobody have shown promising target-to-background ratio (lesion-to-blood 3.3.) in atherosclerotic plaques in mice (Bala *et al.* 2016).

Previously, the same LDLR$^{-/-}$ApoB$^{100/100}$ mouse model and study protocol were applied in a study by Silvola and co-workers using [^{18}F]FDG (Silvola *et al.* 2011). Uptakes of [^{68}Ga]DOTA-Siglec-9 and [^{18}F]FDR-Siglec-9 by aortic plaques, normal vessel wall, and adventitia were similar to those of [^{18}F]FDG. Based on the autoradiography results, the plaque-to-normal vessel wall ratios

were 2.1 ± 0.4 with [68Ga]DOTA-Siglec-9 and 1.9 ± 0.23 with [18F]FDR-Siglec-9. These results were close to the previously reported plaque-to-healthy vessel wall ratio with [18F]FDG (2.2 ± 0.5) (Silvola *et al.* 2011). Low uptake in heart is the major advantage of the radiolabeled Siglec-9 peptide over [18F]FDG.

The uptakes in blood were high in LDLR$^{-/-}$ApoB$^{100/100}$ with both [68Ga]DOTA-Siglec-9 and [18F]FDR-Siglec-9 as compared to [18F]FDG. The serum sVAP-1 is not elevated in all inflammatory diseases (Kurkijärvi *et al.* 1998). However, it has been shown that the sVAP-1 level correlates directly with intima-media thickness and carotid plaques and may be a predictor of early atherosclerosis (Karádi *et al.* 2002; Li *et al.* 2009; Aalto *et al.* 2012, 2014). In Subproject IV, we tried to measure the concentration of VAP-1 but the testing method was not sensitive enough to provide reliable results and therefore it is not clear whether sVAP-1 is the cause for the tracers' high uptake in blood in LDLR$^{-/-}$ApoB$^{100/100}$ mice. Partly, the high blood uptake was caused by the high injected dose, but also the soluble VAP-1 may have played a role. In a rat model with an acute inflammation (Subproject V), blood uptake was much more favorable as compared to the mouse studies. With the LDLR$^{-/-}$ApoB$^{100/100}$ mouse model, the 25 min time point was selected on the basis of the previously reported study (Aalto *et al.* 2011). Because the 68Ga radionuclide emits higher energy positrons (1.90 MeV) with a longer (1.05 mm) range, the 18F-labeled Siglec-9 tracer was used in the Subproject V. 18F emits low energy positron (0.63 MeV) resulting in a shorter positron range (0.27 mm) in soft tissue. However, [18F]FDR-Siglec-9 did not improve the *in vivo* PET image quality in LDLR$^{-/-}$ApoB$^{100/100}$ mice or in the turpentine oil-induced rat model. The limited *in vivo* signal in mice also raises the question whether mouse models are appropriate for preclinical evaluation of new PET tracers as candidates for clinical use. Because mice are not the most ideal model for *in vivo* imaging with PET, the Siglec-9 tracers' usefulness has been evaluated in several experimental animal models. The next step would be the investigation of *in vivo* specificity of [18F]FDR-Siglec-9.

6.5 Future aspects

Nuclear molecular imaging protocols, such as PET, are currently being developed in many areas of medical research and diagnostic practice (Wu *et al.* 2013). PET offers a possibility to visualize, characterize and measure early functional changes before structural damages occur (Mountz, Alavi and Mountz 2012). The non-invasive imaging techniques also allow for early diagnosis, disease monitoring and guidance of treatment strategy. During the past two decades, several molecular imaging protocols have been developed for *in vivo*

detection of inflammation, but as yet, no imaging agent has been found with optimal characteristics to image inflammation (Roivainen, Jalkanen and Nanni 2012).

Many adhesion molecules have been found to contribute to the leukocyte extravasation cascade and are thus attractive targets for detecting inflammation (Wu *et al.* 2013). VAP-1 is involved in many inflammatory diseases, such as RA, atherosclerosis, diabetes and cancer. In normal conditions, VAP-1 is stored in intracellular granules and its luminal expression is upregulated during inflammation. Although VAP-1 plays an important role in the early events of inflammation, its expression on the cell surfaces stays constant for a longer time, if the inflammation sustains. This makes VAP-1 a promising target for both anti-inflammatory therapy and *in vivo* imaging of inflammation (Salmi and Jalkanen 2014).

Our results revealed that Siglec-9/VAP-1 is promising target for molecular imaging of inflammation. The differentiation of aseptic inflammation from bacterial infection is a major diagnostic problem in clinical practise and more specific ECT tracers for detection of bacterial infection are needed. [^{18}F]FDG is not a reliable tracer for differentiation of infection and inflammation (Love, Marwin and Palestro 2009). It would be interesting to investigate [^{18}F]FDR-Siglec-9 in dual time point PET for the detection of peri-implant joint infections in a rat model, because ^{18}F would provide high quality PET images also in late scans ($T_{1/2}$ 110 min) when the contrast between infectious lesions and background may be higher. Siglec-9 is a granulocyte ligand of VAP-1. Granulocytes are the first line immune defense against bacterial infections. The aseptic loosening is not neutrophil mediated and is characterized by poorly vascularized connective tissue dominated mainly fibroblast, macrophages and enhanced osteolysis (Abu-Amer, Darwech and Clohisy 2007). This may affect the luminal expression of VAP-1 and be the factor why Siglec-9/VAP-1 PET could be potential diagnostic candidate for differentiation of aseptic loosening and bacterial infection. Larikka and co-workers showed that late scans could improve diagnostic accuracy of ^{99m}Tc ciprofloxacin in diagnostic imaging (Larikka *et al.* 2002). This would be interesting to test with [^{18}F]FDR-Siglec-9. In addition, the comparison of the results to gold standard WBC imaging would be interesting (Govaert and Glaudemans 2016).

Siglec-9 is a leukocyte ligand of human VAP-1. In mice, Siglec-E is a functional orthologue of human Siglec-9. Siglec-E has not the required arginines, which are crucial for binding to human VAP-1 (Aalto *et al.* 2011). Our radiotracer Siglec-9

contains a short amino acid sequence from human Siglec-9. In these contexts, it would be interesting to investigate further to what extent the differences between Siglecs/SSAO across the species affect, for example, the binding affinity of the tracer. The role of sVAP-1 in different experimental animal models would be also interesting to study, at least considering the target-to-blood ratio in PET imaging studies. The synthetic Siglec-9 has been shown to be a promising tracer for PET imaging of inflammation in several disease models and *in vitro* set ups of human samples. In the future, this novel radiopharmaceutical may potentially be used as a tracer in humans in clinical context. As the first step towards this, first-in-human studies including whole-body distribution, metabolism, plasma pharmacokinetics and dosimetry of [^{68}Ga]DOTA-Siglec-9, will be explored.

7. SUMMARY AND CONCLUSIONS

Our findings support the following conclusions:

1. [^{68}Ga]DOTA-Siglec-9 PET-imaging was able to visualize inflammatory lesions in several experimental animal models

2. [^{68}Ga]DOTA-Siglec-9 uptake was comparable with [^{18}F]FDG in chemically induced synovial inflammation. Synovial inflammation was mild suggesting that [^{68}Ga]DOTA-Siglec-9 could detect synovial inflammation at early stages of the disease.

3. Both [^{68}Ga]DOTA-Siglec-9 and [^{18}F]FDR-Siglec-9 showed similar distribution patterns in a rat model of an acute inflammation and in an atherosclerotic LDLR$^{-/-}$ApoB$^{100/100}$ mouse model

4. VAP-1 plays a role in inflammation-associated atherosclerosis and it is a promising target for anti-inflammatory therapy and *in vivo* imaging.

As a summary, radiolabelled Siglec-9 motif containing peptide(s) targeting VAP-1 can detect inflammation in its early stage and in various pathogeneses. Multimodality *in vivo* imaging facilitates intra-animal comparison and reduces variability of measurements and thus, using PET for preclinical studies, a smaller numbers of animals are needed for obtaining statistically relevant results.

ACKNOWLEDGEMENTS

guidance with IT. I wish to thank our secretary Mirja Jyrkinen and secretary Auli Kärpijoki for all the assistance with paperwork.

It is a privilege to work with such great colleagues as I've had in the pre-clinical group at the Turku PET Centre. I express my gratitude to Johanna, Anu, Miikka, Sanna, Max, Maria, Mia, Petri, Riikka, Jenni, Heidi, Olli, Olli, Juho, Reija, Jussi and Aida for the friendly atmosphere at work. This project has been little bit easier with the shared sense of humor and all the sparkling Fridays.

I sincerely want to thank my dear friends in my life, especially the girls from the senior high-school times, Helena, Laura and Katariina. I also want to thank Maria for being a great friend outside of the office and work as well. I warmly thank all my friends in the field of dog agility, especially for encouraging me to push my limits in exercises and in competitions. You really give a great counterbalance to the work and you are never bored to talk about the dogs and dog sports.

I express my deepest gratitude to my parents Liisa and Mauri Ahtinen for all the support and love during my studies and in life. I also wish to thank my brother Esa Ahtinen for being a friend of a lifetime. I wish to thank my mother-in-law Terttu Virtanen for all the support and encouraging atmosphere. Most of all, I want to thank my beloved husband Juha-Pekka. With your love and support, I managed to complete this study. You have always believed me and my career and made me feel that there are actually several things that I am good at. I love our daily life together and all adventures that we have shared. We share same thoughts and interest about the life. You really are my best friend and soulmate.

Turku, August 2017

Helena Virtanen

REFERENCES

Aalto K, Autio A, Kiss EA et al. Siglec-9 is a novel leukocyte ligand for vascular adhesion protein-1 and can be used in PET imaging of inflammation and cancer. Blood 2011;118:3725–33.

Aalto K, Havulinna AS, Jalkanen S et al. Soluble vascular adhesion protein-1 predicts incident major adverse cardiovascular events and improves reclassification in a finnish prospective cohort study. Circ Cardiovasc Genet 2014;7:529–35.

Aalto K, Maksimow M, Juonala M et al. Soluble vascular adhesion protein-1 correlates with cardiovascular risk factors and early atherosclerotic manifestations. Arterioscler Thromb Vasc Biol 2012;32:523–32.

Abu-Amer Y, Darwech I, Clohisy JC. Aseptic loosening of total joint replacements: mechanisms underlying osteolysis and potential therapies. Arthritis Res Ther 2007;9 Suppl 1:S6.

Airas L, Mikkola J, Vainio JM et al. Elevated Serum Soluble Vascular Adhesion Protein-1 (VAP-1) in Patients with Active Relapsing Remitting Multiple Sclerosis., 2006.

Alt V, Lips KS, Henkenbehrens C et al. A new animal model for implant-related infected non-unions after intramedullary fixation of the tibia in rats with fluorescent in situ hybridization of bacteria in bone infection. Bone 2011;48:1146–53.

An YH, Friedman RJ. Animal models of orthopedic implant infection. J Invest Surg 11:139–46.

An YH, Kang QK, Arciola CR. Animal models of osteomyelitis. Int J Artif Organs 2006;29:407–20.

Anger T, Pohle FK, Kandler L et al. VAP-1, Eotaxin3 and MIG as potential atherosclerotic triggers of severe calcified and stenotic human aortic valves: effects of statins. Exp Mol Pathol 2007;83:435–42.

Aurrand-Lions M, Lamagna C, Dangerfield JP et al. Junctional adhesion molecule-C regulates the early influx of leukocytes into tissues during inflammation. J Immunol 2005;174:6406–15.

Autio A, Henttinen T, Sipilä HJ et al. Mini-PEG spacering of VAP-1-targeting 68Ga-DOTAVAP-P1 peptide improves PET imaging of inflammation. EJNMMI Res 2011;1:10.

Autio A, Saraste A, Kudomi N et al. Assessment of blood flow with (68)Ga-DOTA PET in experimental inflammation: a validation study using (15)O-water. Am J Nucl Med Mol Imaging 2014;4:571–9.

Autio A, Ujula T, Luoto P et al. PET imaging of inflammation and adenocarcinoma xenografts using vascular adhesion protein 1 targeting peptide 68Ga-DOTAVAP-P1: comparison with 18F-FDG. Eur J Nucl Med Mol Imaging 2010;37:1918–25.

Autio A, Vainio PJ, Suilamo S et al. Preclinical evaluation of a radioiodinated fully human antibody for in vivo imaging of vascular adhesion protein-1-positive vasculature in inflammation. J Nucl Med 2013;54:1315–9.

Bailey DL, Willowson KP. Quantitative SPECT/CT: SPECT joins PET as a quantitative imaging modality. Eur J Nucl Med Mol Imaging 2014;41 Suppl 1:S17–25.

Bala G, Blykers A, Xavier C et al. Targeting of vascular cell adhesion molecule-1 by 18F-labelled nanobodies for PET/CT imaging of inflamed atherosclerotic plaques. Eur Heart J Cardiovasc Imaging

2016:jev346 – .

Balato A, Unutmaz D, Gaspari AA. Natural Killer T Cells: An Unconventional T-Cell Subset with Diverse Effector and Regulatory Functions. J Invest Dermatol 2009;129:1628–42.

Barreiro O, Yanez-Mo M, Serrador JM et al. Dynamic interaction of VCAM-1 and ICAM-1 with moesin and ezrin in a novel endothelial docking structure for adherent leukocytes. J Cell Biol 2002;157:1233–45.

Bateman TM. Advantages and disadvantages of PET and SPECT in a busy clinical practice. J Nucl Cardiol 2012;19 Suppl 1:S3–11.

Beck-Broichsitter BE, Smeets R, Heiland M. Current concepts in pathogenesis of acute and chronic osteomyelitis. Curr Opin Infect Dis 2015;28:240–5.

Beer AJ, Kessler H, Wester H-J et al. PET Imaging of Integrin αVβ3 Expression. Theranostics 2011;1:48–57.

Beer AJ, Schwaiger M. Imaging of integrin αvβ3 expression. Cancer Metastasis Rev 2008;27:631–44.

Bhatti M, Chapman P, Peters M et al. Visualising E-selectin in the detection and evaluation of inflammatory bowel disease. Gut 1998;43:40–7.

Blezer ELA, Deddens LH, Kooij G et al. In vivo MR imaging of intercellular adhesion molecule-1 expression in an animal model of multiple sclerosis. Contrast Media Mol Imaging 2015;10:111–21.

Boellaard R, Delgado-Bolton R, Oyen WJG et al. FDG PET/CT: EANM procedure guidelines for tumour imaging: version 2.0. Eur J Nucl Med Mol Imaging 2015;42:328–54.

Bonder CS, Norman MU, Swain MG et al. Rules of recruitment for Th1 and Th2 lymphocytes in inflamed liver: a role for alpha-4 integrin and vascular adhesion protein-1. Immunity 2005;23:153–63.

Branzk N, Papayannopoulos V. Molecular mechanisms regulating NETosis in infection and disease. Semin Immunopathol 2013;35:513–30.

Brooks JL, Jefferson KK. Staphylococcal Biofilms. Advances in Applied Microbiology. Vol 81. 2012, 63–87.

Bulgarelli A, Martins Dias AA, Caramelli B et al. Treatment with methotrexate inhibits atherogenesis in cholesterol-fed rabbits. J Cardiovasc Pharmacol 2012;59:308–14.

Burmester GR, Feist E, Dörner T. Emerging cell and cytokine targets in rheumatoid arthritis. Nat Rev Rheumatol 2013;10:77–88.

Carlos TM, Harlan JM. Leukocyte-endothelial adhesion molecules. Blood 1994;84:2068–101.

Cascão R, Rosário HS, Souto-Carneiro MM et al. Neutrophils in rheumatoid arthritis: More than simple final effectors. Autoimmun Rev 2010;9:531–5.

Cernuda-Morollón E, Ridley AJ. Rho GTPases and leukocyte adhesion receptor expression and function in endothelial cells. Circ Res 2006;98:757–67.

Chaplin DD. Overview of the immune response. J Allergy Clin Immunol 2010;125:S3–23.

Chavakis T, Bierhaus A, Al-Fakhri N et al. The Pattern Recognition Receptor (RAGE) Is a Counterreceptor for Leukocyte Integrins. J Exp Med 2003;198.

Cojocaru M, Cojocaru IM, Silosi I et al. Extra-articular Manifestations in Rheumatoid Arthritis. Maedica (Buchar) 2010;5:286–91.

Crocker PR, Paulson JC, Varki A. Siglecs and their roles in the immune system. Nat Rev Immunol 2007;7:255–66.

Cybulsky MI, Iiyama K, Li H et al. A major role for VCAM-1, but not ICAM-1, in

early atherosclerosis. J Clin Invest 2001;107:1255–62.

Dimastromatteo J, Broisat A, Perret P et al. In vivo molecular imaging of atherosclerotic lesions in ApoE-/- mice using VCAM-1-specific, 99mTc-labeled peptidic sequences. J Nucl Med 2013;54:1442–9.

Dohnt K, Sauer M, Müller M et al. An in vitro urinary tract catheter system to investigate biofilm development in catheter-associated urinary tract infections. J Microbiol Methods 2011;87:302–8.

Dufour EM, Deroche A, Bae Y et al. CD99 is essential for leukocyte diapedesis in vivo. Cell Commun Adhes 2008;15:351–63.

Dunkel P, Balogh B, Meleddu R et al. Semicarbazide-sensitive amine oxidase/vascular adhesion protein-1: a patent survey. Expert Opin Ther Pat 2011;21:1453–71.

Dutta P, Nahrendorf M. Regulation and consequences of monocytosis. Immunol Rev 2014;262:167–78.

von Eiff C, Peters G, Heilmann C. Pathogenesis of infections due to coagulase-negative staphylococci. Lancet Infect Dis 2002;2:677–85.

Enrique-Tarancón G, Castan I, Morin N et al. Substrates of semicarbazide-sensitive amine oxidase co-operate with vanadate to stimulate tyrosine phosphorylation of insulin-receptor-substrate proteins, phosphoinositide 3-kinase activity and GLUT4 translocation in adipose cells. Biochem J 2000;350 Pt 1:171–80.

Eo JS, Jeong JM. Angiogenesis Imaging Using 68Ga-RGD PET/CT: Therapeutic Implications. Semin Nucl Med 2016;46:419–27.

Foot JS, Yow TT, Schilter H et al. PXS-4681A, a Potent and Selective Mechanism-Based Inhibitor of SSAO/VAP-1 with Anti-Inflammatory Effects In Vivo. J Pharmacol Exp Ther 2013;347.

Garrood T, Blades M, Haskard DO et al. A novel model for the pre-clinical imaging of inflamed human synovial vasculature. Rheumatology (Oxford) 2009;48:926–31.

Gent YY, Weijers K, Molthoff CF et al. Evaluation of the novel folate receptor ligand [18F]fluoro-PEG-folate for macrophage targeting in a rat model of arthritis. Arthritis Res Ther 2013;15:R37.

Gent YYJ, Weijers K, Molthoff CFM et al. Promising potential of new generation translocator protein tracers providing enhanced contrast of arthritis imaging by positron emission tomography in a rat model of arthritis. Arthritis Res Ther 2014;16:R70.

Gompels LL, Madden L, Lim NH et al. In vivo fluorescence imaging of E-selectin: Quantitative detection of endothelial activation in a mouse model of arthritis. Arthritis Rheum 2011;63:107–17.

Gordon S, Martinez FO. Alternative Activation of Macrophages: Mechanism and Functions. Immunity 2010;32:593–604.

Govaert GAM, Glaudemans AWJM. Nuclear medicine imaging of posttraumatic osteomyelitis. Eur J Trauma Emerg Surg 2016;42:397–410.

Günther F, Wabnitz GH, Stroh P et al. Host defence against Staphylococcus aureus biofilms infection: Phagocytosis of biofilms by polymorphonuclear neutrophils (PMN). Mol Immunol 2009;46:1805–13.

Hajishengallis G, Chavakis T. Endogenous modulators of inflammatory cell recruitment. Trends Immunol 2013;34:1–6.

Halai K, Whiteford J, Ma B et al. ICAM-2 facilitates luminal interactions between neutrophils and endothelial

cells in vivo. J Cell Sci 2014;127:620–9.

Hansson GK, Hermansson A. The immune system in atherosclerosis. Nat Immunol 2011;12:204–12.

Heemskerk N, van Rijssel J, van Buul JD. Rho-GTPase signaling in leukocyte extravasation. Cell Adh Migr 2014;8:67–75.

Heinonen SE, Leppänen P, Kholová I et al. Increased atherosclerotic lesion calcification in a novel mouse model combining insulin resistance, hyperglycemia, and hypercholesterolemia. Circ Res 2007;101:1058–67.

Hienz SA, Sakamoto H, Flock JI et al. Development and characterization of a new model of hematogenous osteomyelitis in the rat. J Infect Dis 1995;171:1230–6.

Hutchins GD, Miller MA, Soon VC et al. Small animal PET imaging. ILAR J 2008;49:54–65.

Jaakkola K, Nikula T, Holopainen R et al. In vivo detection of vascular adhesion protein-1 in experimental inflammation. Am J Pathol 2000;157:463–71.

Jalkanen S, Karikoski M, Mercier N et al. The oxidase activity of vascular adhesion protein-1 (VAP-1) induces endothelial E- and P-selectins and leukocyte binding. Blood 2007;110:1864–70.

Jalkanen S, Salmi M. Cell surface monoamine oxidases: enzymes in search of a function. EMBO J 2001;20:3893–901.

Jamar F, Buscombe J, Chiti A et al. EANM/SNMMI guideline for 18F-FDG use in inflammation and infection. J Nucl Med 2013;54:647–58.

Karádi I, Mészáros Z, Csányi A et al. Serum semicarbazide-sensitive amine oxidase (SSAO) activity is an independent marker of carotid atherosclerosis. Clin Chim Acta 2002;323:139–46.

Kelly KA, Allport JR, Tsourkas A et al. Detection of vascular adhesion molecule-1 expression using a novel multimodal nanoparticle. Circ Res 2005;96:327–36.

Khalil MM, Tremoleda JL, Bayomy TB et al. Molecular SPECT Imaging: An Overview. Int J Mol Imaging 2011;2011:796025.

Kirsi M, Cheng-Bin Y, Veronica F et al. 64Cu- and 68Ga-Labelled [Nle14,Lys40(Ahx-NODAGA)NH2]-Exendin-4 for Pancreatic Beta Cell Imaging in Rats. Mol Imaging Biol 2014;16:255–63.

Kivi E, Elima K, Aalto K et al. Human Siglec-10 can bind to vascular adhesion protein-1 and serves as its substrate. Blood 2009;114:5385–92.

Kolaczkowska E, Kubes P. Neutrophil recruitment and function in health and inflammation. Nat Rev Immunol 2013;13:159–75.

Komatsu N, Okamoto K, Sawa S et al. Pathogenic conversion of Foxp3+ T cells into TH17 cells in autoimmune arthritis. Nat Med 2013;20:62–8.

Konisti S, Kiriakidis S, Paleolog EM. Hypoxia—a key regulator of angiogenesis and inflammation in rheumatoid arthritis. Nat Rev Rheumatol 2012;8:153–62.

Koort JK, Mäkinen TJ, Knuuti J et al. Comparative 18F-FDG PET of experimental Staphylococcus aureus osteomyelitis and normal bone healing. J Nucl Med 2004;45:1406–11.

Koskinen K, Vainio PJ, Smith DJ et al. Granulocyte transmigration through the endothelium is regulated by the oxidase activity of vascular adhesion protein-1 (VAP-1). Blood 2004;103:3388–95.

Kumar V, Abbas A, Aster JC. Robbins Basic Pathology., 2013.

Kurkijärvi R, Adams DH, Leino R et al. Circulating form of human vascular adhesion protein-1 (VAP-1): increased serum levels in inflammatory liver diseases. J Immunol 1998;161:1549–57.

Kurkijärvi R, Yegutkin GG, Gunson BK et al. Circulating soluble vascular adhesion protein 1 accounts for the increased serum monoamine oxidase activity in chronic liver disease. Gastroenterology 2000;119:1096–103.

Kurosaki T, Kometani K, Ise W. Memory B cells. Nat Rev Immunol 2015;15:149–59.

Kwakman PHS, te Velde AA, Vandenbroucke-Grauls CMJE et al. Treatment and prevention of Staphylococcus epidermidis experimental biomaterial-associated infection by bactericidal peptide 2. Antimicrob Agents Chemother 2006;50:3977–83.

Lacy P. Mechanisms of degranulation in neutrophils. Allergy Asthma Clin Immunol 2006;2:98–108.

van der Laken CJ, Elzinga EH, Kropholler MA et al. Noninvasive imaging of macrophages in rheumatoid synovitis using [11] C-(R)-PK11195 and positron emission tomography. Arthritis Rheum 2008;58:3350–5.

Lalor PF, Sun PJ, Weston CJ et al. Activation of vascular adhesion protein-1 on liver endothelium results in an NF-kappaB-dependent increase in lymphocyte adhesion. Hepatology 2007;45:465–74.

Lambe DW, Ferguson KP, Mayberry-Carson KJ et al. Foreign-body-associated experimental osteomyelitis induced with Bacteroides fragilis and Staphylococcus epidermidis in rabbits. Clin Orthop Relat Res 1991:285–94.

Lankinen P, Lehtimäki K, Hakanen AJ et al. A comparative 18F-FDG PET/CT imaging of experimental Staphylococcus aureus osteomyelitis and Staphylococcus epidermidis foreign-body-associated infection in the rabbit tibia. EJNMMI Res 2012;2:41.

Lankinen P, Mäkinen TJ, Pöyhönen TA et al. 68Ga-DOTAVAP-P1 PET imaging capable of demonstrating the phase of inflammation in healing bones and the progress of infection in osteomyelitic bones. Eur J Nucl Med Mol Imaging 2008;35:352–64.

Larikka MJ, Ahonen AK, Niemelä O et al. Comparison of 99mTc ciprofloxacin, 99mTc white blood cell and three-phase bone imaging in the diagnosis of hip prosthesis infections: improved diagnostic accuracy with extended imaging time. Nucl Med Commun 2002;23:655–61.

Lew DP, Waldvogel FA. Osteomyelitis. N Engl J Med 1997;336:999–1007.

Lew DP, Waldvogel FA. Osteomyelitis. Lancet 2004;364:369–79.

Li H-Y, Jiang Y-D, Chang T-J et al. Serum vascular adhesion protein-1 predicts 10-year cardiovascular and cancer mortality in individuals with type 2 diabetes. Diabetes 2011;60:993–9.

Li H-Y, Lin M-S, Wei J-N et al. Change of serum vascular adhesion protein-1 after glucose loading correlates to carotid intima-medial thickness in non-diabetic subjects. Clin Chim Acta 2009;403:97–101.

Li X, Bauer W, Israel I et al. Targeting P-Selectin by Gallium-68–Labeled Fucoidan Positron Emission Tomography for Noninvasive Characterization of Vulnerable PlaquesSignificance. Arterioscler Thromb Vasc Biol 2014a;34.

Li X-G, Helariutta K, Roivainen A et al. Using 5-deoxy-5-[18F]fluororibose to glycosylate peptides for positron emission tomography. Nat Protoc 2014b;9:138–45.

Li Y-I, Hung J-S, Yu T-Y et al. Serum vascular adhesion protein-1 predicts all-cause mortality and cancer-related mortality in subjects with colorectal cancer. Clin Chim Acta 2014c;428:51–6.

Liaskou E, Karikoski M, Reynolds GM et al. Regulation of mucosal addressin cell adhesion molecule 1 expression in human and mice by vascular adhesion protein 1 amine oxidase activity. Hepatology 2011;53:661–72.

Libby P, DiCarli M, Weissleder R. The vascular biology of atherosclerosis and imaging targets. J Nucl Med 2010;51 Suppl 1:33S – 37S.

Lin P-W, Liu R-S, Liou T-H et al. Correlation between joint [F-18] FDG PET uptake and synovial TNF-alpha concentration: a study with two rabbit models of acute inflammatory arthritis. Appl Radiat Isot 2007;65:1221–6.

Love C, Marwin SE, Palestro CJ. Nuclear Medicine and the Infected Joint Replacement. Semin Nucl Med 2009;39:66–78.

Love C, Palestro CJ. Nuclear medicine imaging of bone infections. Clin Radiol 2016;71:632–46.

Love C, Tomas MB, Tronco GG et al. FDG PET of Infection and Inflammation. RadioGraphics 2005;25:1357–68.

Luster AD, Alon R, von Andrian UH. Immune cell migration in inflammation: present and future therapeutic targets. Nat Immunol 2005;6:1182–90.

Madej A, Reich A, Orda A et al. Expression of vascular adhesion protein-1 in atopic eczema. Int Arch Allergy Immunol 2006;139:114–21.

Mantovani, A, Sica, A, Locati M. Macrophage Polarization Comes of Age. Immunity 2005;23:344–6.

Mantovani A, Garlanda C, Locati M. Macrophage diversity and polarization in atherosclerosis: A question of balance. 2009;29:1419–23.

Marlin SD, Springer TA. Purified intercellular adhesion molecule-1 (ICAM-1) is a ligand for lymphocyte function-associated antigen 1 (LFA-1). Cell 1987;51:813–9.

Martelius T, Salaspuro V, Salmi M et al. Blockade of vascular adhesion protein-1 inhibits lymphocyte infiltration in rat liver allograft rejection. Am J Pathol 2004;165:1993–2001.

Martinez FO, Gordon S. The M1 and M2 paradigm of macrophage activation: time for reassessment. F1000Prime Rep 2014;6:13.

Marttila-Ichihara F, Smith DJ, Stolen C et al. Vascular amine oxidases are needed for leukocyte extravasation into inflamed joints in vivo. Arthritis Rheum 2006;54:2852–62.

Massoud TF, Gambhir SS. Molecular imaging in living subjects: seeing fundamental biological processes in a new light. Genes Dev 2003;17:545–80.

Mayberry-Carson KJ, Tober-Meyer B, Smith JK et al. Bacterial adherence and glycocalyx formation in osteomyelitis experimentally induced with Staphylococcus aureus. Infect Immun 1984;43:825–33.

McEver RP. Selectins: initiators of leucocyte adhesion and signalling at the vascular wall. Cardiovasc Res 2015;107.

McInnes IB, Schett G. Cytokines in the pathogenesis of rheumatoid arthritis. Nat Rev Immunol 2007;7:429–42.

McInnes IB, Schett G. The Pathogenesis of Rheumatoid Arthritis. N Engl J Med 2011;365:2205–19.

Medzhitov R. Origin and physiological roles of inflammation. Nature 2008;454:428–35.

Merinen M, Irjala H, Salmi M et al. Vascular adhesion protein-1 is involved in both acute and chronic inflammation in the mouse. Am J Pathol 2005;166:793–800.

Miese F, Scherer A, Ostendorf B et al. Hybrid 18F-FDG PET–MRI of the hand in rheumatoid arthritis: initial results. Clin Rheumatol 2011;30:1247–50.

Mizuno-Yamasaki E, Rivera-Molina F, Novick P. GTPase networks in membrane traffic. Annu Rev Biochem 2012;81:637–59.

Mountz JM, Alavi A, Mountz JD. Emerging optical and nuclear medicine imaging methods in rheumatoid arthritis. Nat Rev Rheumatol 2012;8:719–28.

Muller WA. Leukocyte–endothelial-cell interactions in leukocyte transmigration and the inflammatory response. Trends Immunol 2003;24:326–33.

Murphy Kenneth, Travers Paul WM. Immuno Biology. 7th ed. Garland Science, Taylor & Francis Group, LLc, 2008.

Murray PJ, Allen JE, Biswas SK et al. Macrophage Activation and Polarization: Nomenclature and Experimental Guidelines. Immunity 2014;41:14–20.

Mäkinen TJ, Lankinen P, Pöyhönen T et al. Comparison of 18F-FDG and 68Ga PET imaging in the assessment of experimental osteomyelitis due to Staphylococcus aureus. Eur J Nucl Med Mol Imaging 2005;32:1259–68.

Nahrendorf M, Jaffer FA, Kelly KA et al. Noninvasive vascular cell adhesion molecule-1 imaging identifies inflammatory activation of cells in atherosclerosis. Circulation 2006;114:1504–11.

Nahrendorf M, Keliher E, Panizzi P et al. 18F-4V for PET–CT Imaging of VCAM-1 Expression in Atherosclerosis. JACC Cardiovasc Imaging 2009;2:1213–22.

Nakamura I, Hasegawa K, Wada Y et al. Detection of early stage atherosclerotic plaques using PET and CT fusion imaging targeting P-selectin in low density lipoprotein receptor-deficient mice. Biochem Biophys Res Commun 2013;433:47–51.

Neut D, C Van Der Mei H, K Bulstra S et al. The role of small-colony variants in failure to diagnose and treat biofilm infections in orthopedics. Acta Orthop 2007;78:299–308.

Noonan T, Lukas S, Peet GW et al. The oxidase activity of vascular adhesion protein-1 (VAP-1) is essential for function. Am J Clin Exp Immunol 2013;2:172–85.

Nourshargh S, Alon R. Leukocyte Migration into Inflamed Tissues. Immunity 2014;41:694–707.

Nourshargh S, Krombach F, Dejana E. The role of JAM-A and PECAM-1 in modulating leukocyte infiltration in inflamed and ischemic tissues. J Leukoc Biol 2006;80:714–8.

O'Rourke AM, Wang EY, Miller A et al. Anti-inflammatory effects of LJP 1586 [Z-3-fluoro-2-(4-methoxybenzyl)allylamine hydrochloride], an amine-based inhibitor of semicarbazide-sensitive amine oxidase activity. J Pharmacol Exp Ther 2008;324:867–75.

O'Rourke AM, Wang EY, Salter-Cid L et al. Benefit of inhibiting SSAO in relapsing experimental autoimmune encephalomyelitis. J Neural Transm 2007;114:845–9.

Otto M. Staphylococcus epidermidis — the "accidental" pathogen. Nat Rev Microbiol 2009;7:555–67.

Packard RRS, Lichtman AH, Libby P. Innate and adaptive immunity in atherosclerosis. Semin Immunopathol 2009;31:5–22.

Palestro CJ. Radionuclide Imaging of Osteomyelitis. Semin Nucl Med 2015;45:32–46.

Panayi GS. Even though T-cell-directed trials have been of limited success, is there reason for optimism? Nat Clin Pract Rheumatol 2006;2:58–9.

Parkin J, Cohen B. An overview of the immune system. Lancet 2001;357:1777–89.

Pettinato C, Sarnelli A, Di Donna M et al. 68Ga-DOTANOC: biodistribution and dosimetry in patients affected by neuroendocrine tumors. Eur J Nucl Med Mol Imaging 2008;35:72–9.

Phillipson M, Kubes P. The neutrophil in vascular inflammation. Nat Med 2011;17:1381–90.

Del Pozo JL, Rouse MS, Euba G et al. The Electricidal Effect Is Active in an Experimental Model of Staphylococcus epidermidis Chronic Foreign Body Osteomyelitis. Antimicrob Agents Chemother 2009;53:4064–8.

Radiation dose to patients from radiopharmaceuticals (addendum 2 to ICRP publication 53). Ann ICRP 1998;28:1–126.

Rahmim A, Zaidi H. PET versus SPECT: strengths, limitations and challenges. Nucl Med Commun 2008;29:193–207.

Retamal J, Sörensen J, Lubberink M et al. Feasibility of (68)Ga-labeled Siglec-9 peptide for the imaging of acute lung inflammation: a pilot study in a porcine model of acute respiratory distress syndrome. Am J Nucl Med Mol Imaging 2016;6:18–31.

Roivainen A, Jalkanen S, Nanni C. Gallium-labelled peptides for imaging of inflammation. Eur J Nucl Med Mol Imaging 2012;39 Suppl 1:S68–77.

Roivainen A, Parkkola R, Yli-Kerttula T et al. Use of positron emission tomography with methyl-^{11}C-choline and 2-^{18}F-fluoro-2-deoxy- D - glucose in comparison with magnetic resonance imaging for the assessment of inflammatory proliferation of synovium. Arthritis Rheum 2003;48:3077–84.

Rosado-de-Castro PH, Lopes de Souza SA, Alexandre D et al. Rheumatoid arthritis: Nuclear Medicine state-of-the-art imaging. World J Orthop 2014;5:312–8.

Rosales C, Demaurex N, Lowell CA et al. Neutrophils: Their Role in Innate and Adaptive Immunity. J Immunol Res 2016;2016:1469780.

Rossin R, Muro S, Welch MJ et al. In vivo imaging of 64Cu-labeled polymer nanoparticles targeted to the lung endothelium. J Nucl Med 2008;49:103–11.

Rouzet F, Bachelet-Violette L, Alsac J-M et al. Radiolabeled fucoidan as a p-selectin targeting agent for in vivo imaging of platelet-rich thrombus and endothelial activation. J Nucl Med 2011;52:1433–40.

Sadat U, Jaffer FA, van Zandvoort MAMJ et al. Inflammation and neovascularization intertwined in atherosclerosis: imaging of structural and molecular imaging targets. Circulation 2014;130:786–94.

Sadik CD, Kim ND, Luster AD. Neutrophils cascading their way to inflammation. Trends Immunol 2011;32:452–60.

Sakaeda H. [Experimental polymicrobial osteomyelitis produced by both aerobic and anaerobic opportunistic pathogens]. Nihon Seikeigeka Gakkai Zasshi 1988;62:791–802.

Salmi M, Jalkanen S. A 90-kilodalton endothelial cell molecule mediating lymphocyte binding in humans. Science 1992;257:1407–9.

Salmi M, Jalkanen S. VAP-1: an adhesin and an enzyme. Trends Immunol 2001;22:211–6.

Salmi M, Jalkanen S. Ectoenzymes controlling leukocyte traffic. Eur J Immunol 2012;42:284–92.

Salmi M, Jalkanen S. Ectoenzymes in leukocyte migration and their therapeutic potential. Semin Immunopathol 2014;36:163–76.

Salmi M, Kalimo K, Jalkanen S. Induction and function of vascular adhesion protein-1 at sites of inflammation. J Exp Med 1993;178:2255–60.

Salmi M, Stolen C, Jousilahti P et al. Insulin-regulated increase of soluble vascular adhesion protein-1 in diabetes. Am J Pathol 2002;161:2255–62.

Salter-Cid LM, Wang E, O'Rourke AM et al. Anti-inflammatory effects of inhibiting the amine oxidase activity of semicarbazide-sensitive amine oxidase. J Pharmacol Exp Ther 2005;315:553–62.

Sanchez-Crespo A. Comparison of Gallium-68 and Fluorine-18 imaging characteristics in positron emission tomography. Appl Radiat Isot 2013;76:55–62.

Sansbury BE, Spite M. Resolution of Acute Inflammation and the Role of Resolvins in Immunity, Thrombosis, and Vascular Biology. Circ Res 2016;119:113–30.

Schenkel AR, Mamdouh Z, Chen X et al. CD99 plays a major role in the migration of monocytes through endothelial junctions. Nat Immunol 2002;3:143–50.

Schett G, Gravallese E. Bone erosion in rheumatoid arthritis: mechanisms, diagnosis and treatment. Nat Rev Rheumatol 2012;8:656–64.

Schilter HC, Collison A, Russo RC et al. Effects of an anti-inflammatory VAP-1/SSAO inhibitor, PXS-4728A, on pulmonary neutrophil migration. Respir Res 2015;16:42.

Schnöckel U, Hermann S, Stegger L et al. Small-animal PET: A promising, non-invasive tool in pre-clinical research. Eur J Pharm Biopharm 2010;74:50–4.

Sharon N, Lis H. History of lectins: from hemagglutinins to biological recognition molecules. Glycobiology 2004;14:53R – 62R.

Silvola J, Autio A, Luoto P et al. Preliminary evaluation of novel ^{68}Ga-DOTAVAP-PEG-P2 peptide targeting vascular adhesion protein-1. Clin Physiol Funct Imaging 2010;30:75–8.

Silvola JMU, Saraste A, Laitinen I et al. Effects of age, diet, and type 2 diabetes on the development and FDG uptake of atherosclerotic plaques. JACC Cardiovasc Imaging 2011;4:1294–301.

Solé M, Hernandez-Guillamon M, Boada M et al. p53 phosphorylation is involved in vascular cell death induced by the catalytic activity of membrane-bound SSAO/VAP-1. Biochim Biophys Acta - Mol Cell Res 2008;1783:1085–94.

Sovijärvi Anssi, Ahonen Aapo, Hartiala Jaakko, Länsimies Esko, Savolainen Sauli, Turjanmaa Väinö VE. Kliininen Fysiologia Ja Isotooppilääketiede. 1. painos. Helsinki: Kustannus Oy Duodecim, 2003.

Stolen CM, Yegutkin GG, Kurkijärvi R et al. Origins of Serum Semicarbazide-Sensitive Amine Oxidase. Circ Res 2004;95.

Stumpe KDM, Nötzli HP, Zanetti M et al. FDG PET for Differentiation of Infection and Aseptic Loosening in Total Hip Replacements: Comparison with Conventional Radiography and Three-Phase Bone Scintigraphy. Radiology 2004;231:333–41.

Swirski FK, Nahrendorf M. Leukocyte behavior in atherosclerosis, myocardial infarction, and heart failure. Science 2013;339:161–6.

Szekanecz Z, Pakozdi A, Szentpetery A et al. Chemokines and angiogenesis in rheumatoid arthritis. Front Biosci

(Elite Ed) 2009;1:44–51.

Teng Z, He J, Degnan AJ et al. Critical mechanical conditions around neovessels in carotid atherosclerotic plaque may promote intraplaque hemorrhage. Atherosclerosis 2012;223:321–6.

Ter-Pogossian MM, Phelps ME, Hoffman EJ et al. A positron-emission transaxial tomograph for nuclear imaging (PETT). Radiology 1975;114:89–98.

Tohka S, Laukkanen M, Jalkanen S et al. Vascular adhesion protein 1 (VAP-1) functions as a molecular brake during granulocyte rolling and mediates recruitment in vivo. FASEB J 2001;15:373–82.

Toiyama Y, Miki C, Inoue Y et al. Circulating form of human vascular adhesion protein-1 (VAP-1): decreased serum levels in progression of colorectal cancer and predictive marker of lymphatic and hepatic metastasis. J Surg Oncol 2009;99:368–72.

Trentham DE, Townes AS, Kang AH. Autoimmunity to type II collagen an experimental model of arthritis. J Exp Med 1977;146:857–68.

Udalova IA, Mantovani A, Feldmann M. Macrophage heterogeneity in the context of rheumatoid arthritis. Nat Rev Rheumatol 2016;12:472–85.

Ujula T, Salomäki S, Virsu P et al. Synthesis, 68Ga labeling and preliminary evaluation of DOTA peptide binding vascular adhesion protein-1: a potential PET imaging agent for diagnosing osteomyelitis. Nucl Med Biol 2009;36:631–41.

Wang S, Xiang S, Wu X et al. Regulation of Macrophage Polarization During Atherosclerosis. Lipid Cardiovasc Res 2016;2:05–12.

Ward ST, Weston CJ, Shepherd EL et al. Evaluation of serum and tissue levels of VAP-1 in colorectal cancer. BMC

Cancer 2016;16:154.

Watson RL, Buck J, Levin LR et al. Endothelial CD99 signals through soluble adenylyl cyclase and PKA to regulate leukocyte transendothelial migration. J Exp Med 2015;212.

Wehrl HF, Judenhofer MS, Wiehr S et al. Pre-clinical PET/MR: technological advances and new perspectives in biomedical research. Eur J Nucl Med Mol Imaging 2009;36 Suppl 1:S56–68.

Weiner RE, Sasso DE, Gionfriddo MA et al. Early detection of bleomycin-induced lung injury in rat using indium-111-labeled antibody directed against intercellular adhesion molecule-1. J Nucl Med 1998;39:723–8.

Weston CJ, Shepherd EL, Claridge LC et al. Vascular adhesion protein-1 promotes liver inflammation and drives hepatic fibrosis. J Clin Invest 2015;125:501–20.

Vestweber D, Blanks JE. Mechanisms That Regulate the Function of the Selectins and Their Ligands. Physiol Rev 1999;79.

Vestweber D. How leukocytes cross the vascular endothelium. Nat Rev Immunol 2015;15:692–704.

Wilder RL. Integrin alpha V beta 3 as a target for treatment of rheumatoid arthritis and related rheumatic diseases. Ann Rheum Dis 2002;61 Suppl 2:ii96–9.

De Winter F, Vogelaers D, Gemmel F et al. Promising Role of 18-F-Fluoro-D-Deoxyglucose Positron Emission Tomography in Clinical Infectious Diseases. Eur J Clin Microbiol Infect Dis 2002;21:247–57.

Vivier E, Ugolini S, Blaise D et al. Targeting natural killer cells and natural killer T cells in cancer. Nat Rev Immunol 2012;12:239–52.

Volk A, Crémieux AC, Belmatoug N et al.

Evaluation of a rabbit model for osteomyelitis by high field, high resolution imaging using the chemical-shift-specific-slice-selection technique. Magn Reson Imaging 1994;12:1039–46.

Woodfin A, Reichel CA, Khandoga A et al. JAM-A mediates neutrophil transmigration in a stimulus-specific manner in vivo: evidence for sequential roles for JAM-A and PECAM-1 in neutrophil transmigration. Blood 2007;110:1848–56.

Woollard KJ, Geissmann F. Monocytes in atherosclerosis: subsets and functions. Nat Rev Cardiol 2010;7:77–86.

Wu C, Li F, Niu G et al. PET imaging of inflammation biomarkers. Theranostics 2013;3:448–66.

Xue J, Schmidt SV, Sander J et al. Transcriptome-Based Network Analysis Reveals a Spectrum Model of Human Macrophage Activation. Immunity 2014;40:274–88.

Yamada S, Kubota K, Kubota R et al. High accumulation of fluorine-18-fluorodeoxyglucose in turpentine-induced inflammatory tissue. J Nucl Med 1995;36:1301–6.

Yoo TJ, Kim SY, Stuart JM et al. Induction of arthritis in monkeys by immunization with type II collagen. J Exp Med 1988;168:777–82.

Zhang JQ, Nicoll G, Jones C et al. Siglec-9, a novel sialic acid binding member of the immunoglobulin superfamily expressed broadly on human blood leukocytes. J Biol Chem 2000;275:22121–6.

Zhu Z, Yin Y, Zheng K et al. Evaluation of synovial angiogenesis in patients with rheumatoid arthritis using ^{68}Ga-PRGD2 PET/CT: a prospective proof-of-concept cohort study. Ann Rheum Dis 2014;73:1269–72.

Zimmerli W, Trampuz A, Ochsner PE. Prosthetic-Joint Infections. N Engl J Med 2004;351:1645–54.